1.E.2:
1.D.4

Nuclear Physics **81** (1966) 1—60; © *North-Holland Publishing Co., Amsterdam*

NUCLEAR MASSES AND DEFORMATIONS

WILLIAM D. MYERS and WLADYSLAW J. SWIATECKI

Lawrence Radiation Laboratory, University of California, Berkeley, California†

Received 7 September 1965

Abstract: A semi-empirical theory of nuclear masses and deformations is presented. The potential energy of a nucleus, considered as a function of N, Z and the nuclear shape, is assumed to be given by the liquid-drop model, modified by a shell correction. The shell correction is a simple function of N and Z and is supposed to disappear as the nucleus is distorted away from the spherical shape. The resulting semi-empirical expression for the nuclear deformation energy has seven adjustable parameters, four in the liquid-drop part and three in the shell correction. By making the deformation energy stationary with respect to distortions, the equilibrium deformations (i.e., the quadrupole moments) and the ground-state masses of nuclei are derived as functions of N and Z. In addition, from unstable shapes of equilibrium corresponding to saddle-point configurations, barrier energies for nuclear fission are deduced. The predictions of the theory are compared with some 1200 experimental nuclear masses, 240 quadrupole moments and 40 fission barriers. The results lead, on the one hand, to a re-assessment of the accuracy of the liquid-drop model and a firmer determination of its characteristic constants and, on the other, to a semi-quantitative understanding of the effects of shell structure on nuclear masses and deformations. A number of minor anomalies are isolated, one apparently related to the so-called Wigner term in the binding energy and one relevant for the understanding of fission barriers. Applications to the analysis of the centrifugal stretching of nuclei and to the possible existence of "islands of stability" in the region of super-heavy nuclei are mentioned.

CONTENTS

1. Introduction 2
2. Qualitative considerations 4
3. The shell function $S(N, Z)$ 7
   3.1 Complete bunching 7
   3.2 Incomplete bunching 11
   3.3 Potential energy and its velocity dependence 11
   3.4 Predominant sign of ΔE 12
4. The deformability of nuclei and the attenuating function 13
5. The mass formula 21
6. Fitting of adjustable parameters 28
   6.1 Determination of liquid-drop parameters 29
   6.2 Determination of shell-correction parameters 32
7. Discussion of results 35
   7.1 Smooth trends 36
   7.2 The Wigner term 37
   7.3 Shell function for $N, Z \leqq 29$ 40
   7.4 Heavy-element anomaly 44

† This work was done largely under the auspices of the U.S. Atomic Energy Commission; one of the authors (W.D.M.) also wishes to acknowledge the National Science Foundation for support during part of this research.

7.5 Rare-earth anomaly 44
7.6 Quadrupole moments 45
7.7 Fission barriers 45
7.8 Super-heavy nuclei 49
7.9 Centrifugal stretching of nuclei 51
7.10 How to use the mass formula 51
8. Summary and conclusions 52
Appendices 54
A.1. Details of equilibrium deformations 54
A.2. Diffuseness and curvature corrections 57
A.3. Fold-out figures 59
References 59

1. Introduction

This paper is the result of an attempt to gain a simple understanding of the principal effects of shell structure on the masses and equilibrium configurations of nuclei †.

Apart from shell effects, a good representation of the trends in nuclear masses may be obtained by using the model of a charged liquid drop possessing a surface tension (see fig. 1 and ref. [1])). The stable equilibrium shapes predicted by this model are spherical. In recent years a vast amount of information has been accumulated on the details of the deviations of nuclear masses from a smooth liquid-drop formula and on the deviations of nuclear shapes from a sphere. The nature of the deviations of the masses is illustrated in figs. 21(a) and 22(a) in appendix A.3. We note the dips in the mass deviations for nuclei with magic numbers of neutrons or protons, and the rise and fall of the masses between magic numbers. This rise and fall is sometimes fairly smooth (e.g., between the magic numbers N or $Z = 28$ and 50, and between $N = 50$ and 82), and sometimes it is interrupted by an approximate flattening-out of the mass deviations. This occurs in the region of the rare earths ($N \approx 88$ to $N \approx 112$) and again for heavy nuclei ($N \geqq 136$). It is also in these regions of the periodic table that strongly deformed nuclei are observed, stable ground state deformations appearing and disappearing in the neighbourhood of the above neutrons numbers (see fig. 23(a) in appendix A.3). These features are associated with nuclear shell structure, and both qualitative considerations and detailed studies of individual nuclei have been reported that attempt to relate the observations to the details of nuclear level diagrams and to the competition between long-range and pairing forces in nuclei (see, for example, refs. [2-4])).

In the present paper we shall aim at a semi-quantitative account of the two principal features of the experimental trends (bumps in the mass deviations between magic numbers and flattened bumps accompanied by deformations) in terms of a primitive semi-empirical theory of nuclear masses based on two physical ingredients:

† The present paper is part of a University of California Lawrence Radiation Laboratory report, UCRL-11980, which also contains a table of nuclear properties based on the theory developed here.

(i) The bumps in the masses are associated with a "bunching" of energy levels in a spherical nuclear potential, the filling of a bunch corresponding to a closed-shell configuration.

(ii) The above bunching, being associated with the spherical shape of the nuclear potential, will disappear for a sufficiently distorted configuration.

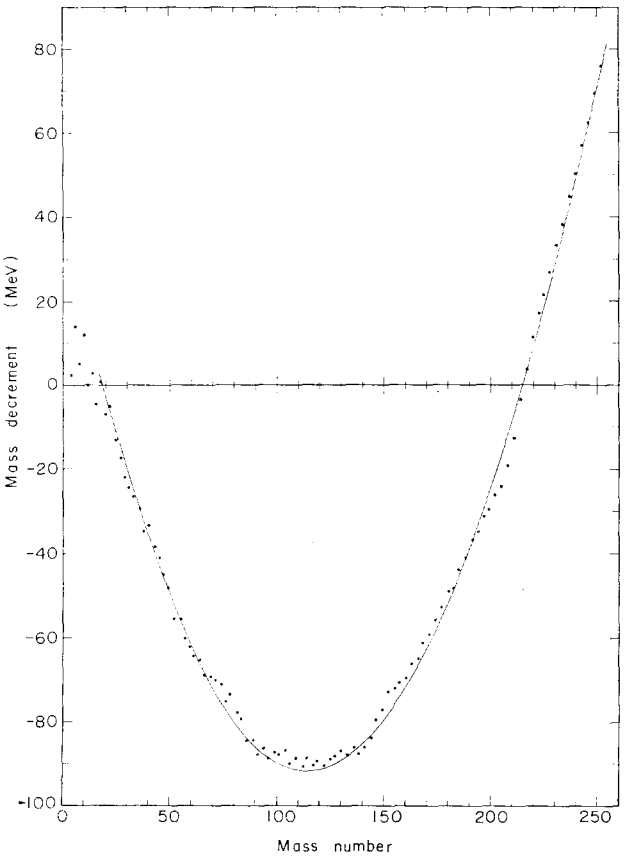

Fig. 1. The mass decrements of 97 beta-stable nuclei are compared with the smooth curve corresponding to the liquid-drop part of our mass formula. Note that the over-all trend of the decrements is reproduced throughout the periodic table, including the light nuclei. The scatter of the points is due to shell effects.

The first of these ingredients underlies the work of Mozer [5]) on nuclear masses, and, with a more detailed specification of the bunching of levels, also the recent work of Kümmel *et al.* [6]).

The second ingredient expresses the requirement that for very distorted nuclear shapes the bunching of levels characteristic of the known magic numbers would be destroyed owing to the removal of degeneracies associated with the spherical shape.

We shall formalize the above two requirements by writing down a correction to the liquid-drop formula for the mass of a nucleus (a function of N, Z and the nuclear shape), the correction being such a function of N and Z as to embody the first requirement, and such a function of shape as to embody the second requirement. (The second requirement is simply the vanishing of the correction for large distortions).

The resulting expression for the mass of a nucleus will be, like the original liquid-drop formula, a function of N, Z and *shape*. In this sense it will be more than a mass formula, aiming to reproduce only the experimental nuclear masses. It will be a semi-empirical theory of the nuclear potential energy considered as a function of deformation. As a result, by minimizing the mass with respect to the shape, we will be able to deduce, in addition to the ground state masses of nuclei, also their equilibrium deformations. Furthermore, a discussion of the distortion energy in nuclear fission, in particular of the fission barriers, will be possible.

The plan of this paper is as follows: In sect. 2 we explain briefly the qualitative features of the mass formula. In sects. 3 and 4 we go through the derivation of the functional form of the shell correction. This enables us to present in sect. 5 the detailed appearance of the mass formula and to derive analytical expressions for the predicted masses and deformations of nuclei. Sect. 6 explains how the adjustable parameters were fitted from experimental data. Sect. 7 discusses in ten subsections various results following from our semi-empirical theory. Sect. 8 summarizes the paper.

2. Qualitative Considerations

The semi-empirical mass equation, whose derivation will be explained in sects. 3–5, has the following form:

$$\begin{aligned} M(N, Z, \text{shape}) &= M_{\text{liquid drop}} + M_{\text{shells}} \\ &= M_{\text{liquid drop}}(N, Z, \text{shape}) \\ &\quad + Cs(N, Z)\mathrm{e}^{-(\text{distortion})^2/a^2}. \end{aligned} \tag{1}$$

The last term is the shell correction and is a product of an over-all amplitude factor C, a dimensionless function $s(N, Z)$ and an attenuating factor exp[-(distortion)$^2/a^2$] of range a. The function $s(N, Z)$, one form of which will be derived in sect. 3, has the general appearance of negative dips at magic numbers, with positive bumps in between. The attenuating factor makes the whole shell correction disappear with increasing distortion of the nucleus. The "distortion" in eq. (1) is the root-mean-square value of the deviation of the radius vector $R(\theta, \phi)$, specifying the nuclear surface, from its average value R_0; i.e.,

$$(\text{distortion})^2 \equiv \overline{(\delta R)^2} = \frac{\iint \mathrm{d}\Omega (R - R_0)^2}{\iint \mathrm{d}\Omega},$$

the integrations being over the solid angle 4π. The Gaussian form of the attenuating factor is discussed in sect. 4.

For a spherical shape $\overline{(\delta R)^2}$ is zero and the shell correction is $Cs(N, Z)$, which we shall denote by $S(N, Z)$. The function $S(N, Z)$ thus represents what the effects of

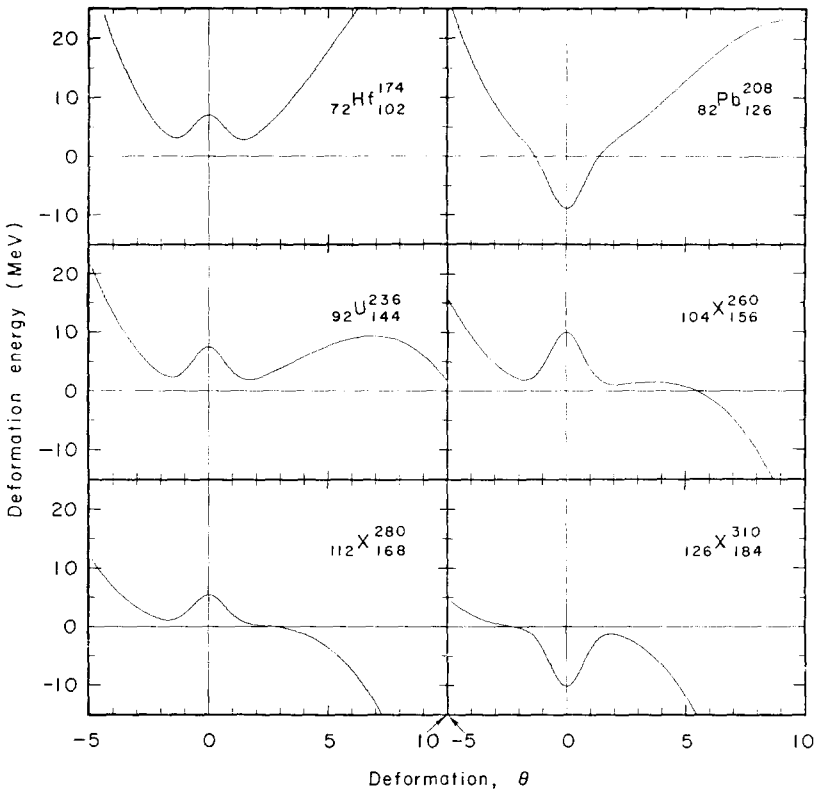

Fig. 2. The deformation energy deduced from our mass formula is shown in its dependence on a deformation parameter θ (a measure of the eccentricity of the spheroidal nuclear shapes). The case of ^{174}Hf illustrates how a positive Gaussian bump, representing shell effects, when superimposed on a liquid-drop restoring potential, leads to a stable prolate equilibrium shape. (The oblate shape, corresponding to negative θ, is unstable with respect to ellipsoidal distortions not displayed in this figure.) The case of ^{208}Pb shows how a negative Gaussian bump leads to a relatively undeformable closed-shell configuration, with an anomalously high fission barrier. (The barrier shown in this figure is somewhat higher than our formula actually predicts, because all the graphs were obtained – for ease of illustration – from an approximation valid only for moderate θ values. See appendix A.1.) The case of ^{236}U shows the effect of a positive bump in lowering the fission barrier, which in the next two cases ($A = 260$ and $A = 280$) leads to nuclei virtually unstable against fission. The case of $A = 310$ illustrates a nucleus that has been stabilized against fission by a hypothetical doubly magic number at $N = 184, Z = 126$.

shells would be in a nucleus whose shape was forced to be spherical. The shape dependence of the shell correction is contained in the factor $\exp[-\overline{(\delta R)^2}/a^2]$.

The precise form of the liquid-drop part of the mass formula is not of importance for the present qualitative discussion. In developing our mass formula we first considered a conventional liquid-drop expression consisting of volume, surface and

electrostatic energies (and an even-odd correction), but we later incorporated one or two refinements.

Without going into the details of either the liquid-drop part of the mass formula or of the precise form of the shell function $S(N, Z)$, we may deduce the principal qualitative consequences of the expression (1) that follow from the fact that the shell correction $S(N, Z)$ changes from generally negative values in the vicinity of magic numbers to generally positive values in between.

We note that the liquid-drop formula predicts a stable spherical equilibrium shape for a nucleus and that, according to eq. (1), this is still the case when the shell function $S(N, Z)$ is negative. The result of using eq. (1) in the vicinity of the closed shells is, therefore, a spherical nucleus with unusual stability (see the curve for ^{208}Pb in fig. 2). On the other hand if, between magic numbers, $S(N, Z)$ should become sufficiently positive, the stabilizing tendency of the liquid-drop part of the mass formula will be overcome by the opposite tendency of the shell correction, and the spherical shape will become unstable. Since, however, the shell correction is assumed to disappear for large distortions, the decrease in mass will only continue up to about the range a of the attenuating function, after which the liquid-drop part will take over and the mass will, once again, increase. (We are disregarding the possibility of fission, which will be considered later). The result will then be a stable, non-spherical configuration – see the curve for ^{174}Hf in fig. 2. From this figure it may also be deduced that, according to eq. (1), the mass of a nucleus in the deformed configuration is less than the sum of the liquid-drop mass and the shell correction for the *spherical* configuration. Since this latter quantity, considered as a function of N and Z, has the appearance of bumps between magic numbers, the transition from spherical to non-spherical equilibrium shapes will be accompanied by a flattening-out of the bumps.

These qualitative features follow from the form of eq. (1). It is possible to go somewhat further without specifying more closely the function $S(N, Z)$. The general theory of the "exchange of stabilities" between different families of equilibrium configurations of a system (see, for example, refs. [7-9]) shows that at the moment when the nature of the equilibrium of the sphere changes from stable to unstable with the increase of S above a critical value S_{crit} the resulting stable deformations are, at first, proportional to $\pm(S-S_{crit})^{\frac{1}{2}}$. (For details see appendix 1). This means that the deformations come in abruptly, with a vertical tangent, when plotted as a function of the excess over the critical condition. Similarly, when in the second half of a shell, S is about to decrease below S_{crit} the deformations will disappear abruptly with a vertical tangent.

On the other hand, with the finite-range attenuating function assumed in eq. (1), the stable deformations will only very slowly – logarithmically – exceed in order of magnitude the range of the attenuating function, once the value of S has exceeded appreciably the critical value. The result is then that the mass formula (1) will predict deformations appearing and disappearing suddenly at certain critical points between magic numbers and fairly constant in between.

We note finally that since stable deformations will appear only if the shell function $S(N, Z)$ exceeds a certain minimum value, sufficient to overcome the stabilizing effect of the liquid-drop part of eq. (1), deformations will not, in general, be found between all magic numbers. They will be most likely to appear either when S is particularly large (regions of the periodic table away from magic neutron or proton numbers), or when the liquid-drop stabilizing effect is small (region of heavy nuclei).

These qualitative features, which follow more or less directly from our two physical assumptions, appear to bear some resemblance to the experimental behaviour of nuclear masses and deformations, and we shall examine in sect. 7 the degree of quantitative agreement that may be attained using a particularly simple form of $S(N, Z)$, which we shall now derive.

3. The Shell Function $S(N, Z)$

We shall derive an expression for the shell correction $\Delta E = S(N, Z)$ by considering it to be the result of the bunching of an originally smooth distribution of single-particle levels into one that consists of groups of levels corresponding to the observed magic numbers. The shell correction will be taken to be the difference between a sum over single-particle contributions in the bunched and unbunched situations:

$$\Delta E = \sum \varepsilon_i(\text{bunched}) - \sum \varepsilon_i(\text{unbunched}), \tag{2}$$

where ε_i are the single-particle contributions to the total energy. The spectrum of these single-particle contributions could be chosen with varying degrees of refinement, an extreme approach being one in which it was made to correspond as closely as possible with single-particle levels in a nuclear potential of the type studied by Nilsson [10]). Another, purely empirical, approach would be to specify the level spectrum by means of a large number of adjustable parameters, to be fixed with reference to the experimental masses [6]). In this paper, aimed at the greatest possible simplicity, we shall consider the case in which the unbunched level spectrum in eq. (2) corresponds to that of an ideal degenerate Fermi gas, and the bunched spectrum results from cutting up the smooth spectrum into groups, with populations corresponding to the sizes of shells between magic numbers, and then compressing each group so as to produce a series of bands with gaps at magic numbers.

3.1. COMPLETE BUNCHING

Consider first the extreme case in which the bands are completely bunched into degenerate levels whose positions are specified by $t_1, t_2 \cdots t_i \cdots$ as reckoned from the bottom of the potential well (see fig. 3). A nucleus is thus supposed to consist of neutrons and protons, each with its bunched spectrum of levels (these could be different for the neutrons and protons). The size of the well – the same for neutrons and protons – is assumed to be proportional to the total number of particles, A

(equal to $N+Z$). This means that for nuclei with $N = Z = \frac{1}{2}A$, the smooth Fermi gas would fill the well to a constant depth, independent of A and equal to the Fermi energy t_F of a "standard nucleus". [This is related to the nuclear radius constant r_0 by $t_F = (\frac{9}{8}\pi)^{\frac{2}{3}}(\hbar^2/2Mr_0^2)$, where M is the nucleon mass.] The maximum energies of the Fermi gases representing the neutrons and protons in the unbunched case are

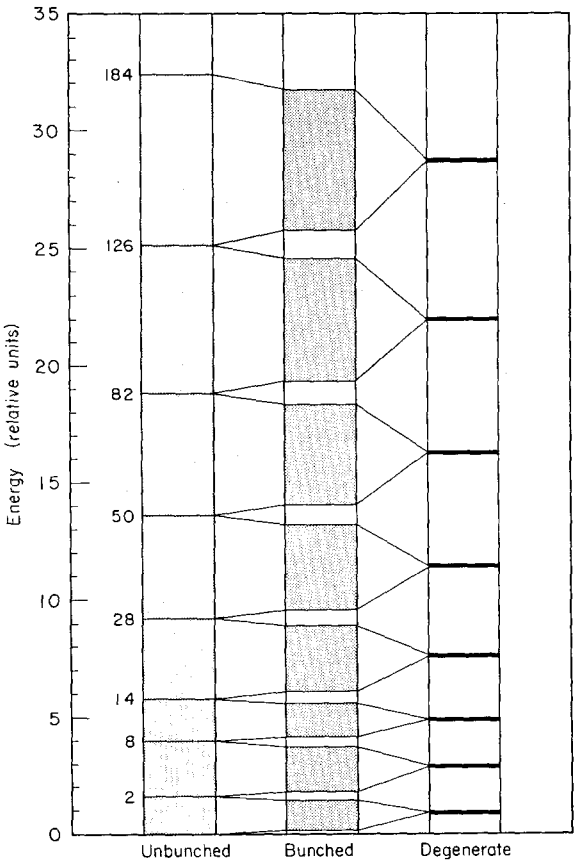

Fig. 3. Schematic diagram of a Fermi-gas spectrum of levels (on the left), cut up into bands corresponding to magic numbers, and bunched. The degree of bunching is 100% on the right and 17.5% in the centre; this is the degree of bunching deduced from experiment.

then $t_N = t_F(N/\frac{1}{2}A)^{\frac{2}{3}}$ and $t_Z = t_F(Z/\frac{1}{2}A)^{\frac{2}{3}}$, according to the proportionality of the kinetic energy to the two-thirds power of the particle number for a Fermi gas. From this proportionality it also follows that the energy of the nth neutron in a well of fixed size (i.e., for a given A) is given by t, where

$$\frac{t}{t_N} = \left(\frac{n}{N}\right)^{\frac{2}{3}},$$

and the total (kinetic) energy of all N neutrons in the unbunched case is given by

$$\int_0^N t\,\mathrm{d}n = \frac{t_N}{N^{\frac{2}{3}}}\int_0^N n^{\frac{2}{3}}\,\mathrm{d}n. \tag{3}$$

(We shall use integrals instead of sums since the discreteness of particles will be disregarded.)

In the bunched case (see fig. 3) all levels between M_{i-1} and M_i are at the same energy t_i, and all particles between M_{i-1} and M_i are therefore contributing at a constant rate in the integration from $n = 0$ to $n = N$; the rate of contribution, regarded as a function of n, is a series of constants t_i, one for each shell. We may consequently write the total energy of the neutrons in the bunched case as an integral from zero to N over a "staircase function" $t_{\text{staircase}}(n)$, consisting of steps of constant height t_i between magic numbers. Introducing a dimensionless staircase function $q(n)$ defined in terms of $t_{\text{staircase}}(n)$ through

$$t_{\text{staircase}}(n) = \frac{t_N}{N^{\frac{2}{3}}}\,q(n),$$

we may write the total neutron kinetic energy in the bunched case in a way analogous to eq. (3) as

$$\frac{t_N}{N^{\frac{2}{3}}}\int_0^N q(n)\mathrm{d}n,$$

where

$$q(n) = q_i = \frac{N^{\frac{2}{3}}}{t_N}\,t_i \qquad \text{for} \quad M_{i-1} < n < M_i.$$

The difference in energy between the bunched and unbunched cases (associated with the neutrons) is then

$$\frac{t_N}{N^{\frac{2}{3}}}\int_0^N [q(n) - n^{\frac{2}{3}}]\mathrm{d}n.$$

Considering the protons in the well to be bunched like the neutrons the total kinetic energy difference between the bunched and unbunched cases may be written as

$$\Delta E = \frac{t_N}{N^{\frac{2}{3}}}\,F(N) + \frac{t_Z}{Z^{\frac{2}{3}}}\,F(Z) = t_{\mathrm{F}}\,\frac{F(N)+F(Z)}{(\frac{1}{2}A)^{\frac{2}{3}}}, \tag{4}$$

where

$$F(N) = \int_0^N [q(n) - n^{\frac{2}{3}}]\mathrm{d}n.$$

At this stage various degrees of refinement are still possible in the choice of the staircase function $q(n)$. For example all the levels t_i, and consequently all the values

q_i, might be regarded as adjustable parameters, possibly different for neutrons and protons. This, although a plausible approach in a purely empirical description of nuclear masses, introduces rather more freedom than is necessary, because a completely arbitrary distribution of the values t_i would include systems bearing no resemblance whatever to a nucleus of approximately constant density and constant energy per particle. If the system represented by the bunched spectrum is to bear some resemblance to nuclei, the levels t_i should remain in the general neighbourhood of the unbunched bands that they are supposed to represent. One possible idealization is to put each t_i at the average position (i.e., at the centre of gravity) of the unbunched band that it represents. This prescription would imply that q_i is the average value of $n^{\frac{2}{3}}$ between $n = M_{i-1}$ and $n = M_i$, or, explicitly

$$q_i = \frac{\int_{M_{i-1}}^{M_i} n^{\frac{2}{3}} \mathrm{d}n}{\int_{M_{i-1}}^{M_i} \mathrm{d}n} = \frac{3}{5} \frac{M_i^{\frac{5}{3}} - M_{i-1}^{\frac{5}{3}}}{M_i - M_{i-1}}.$$

This choice of q_i specifies completely one form of the shell correction – see fig. 4. The resulting expression for ΔE, considered as a function of N and Z, has the appearance of cushion-like bumps between lines corresponding to the magic numbers.

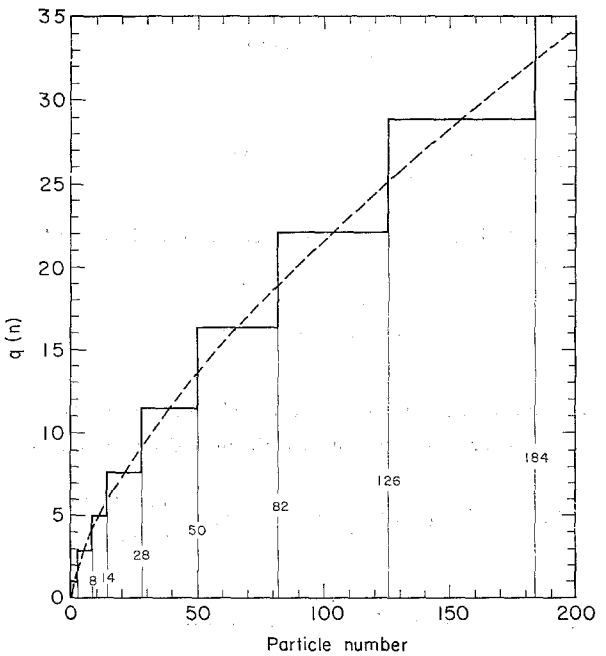

Fig. 4. The staircase function $q(n)$ is compared with the smooth function $n^{\frac{2}{3}}$ (the dashed curve). The difference between the two functions, when integrated up to N or Z, gives the shell function $F(N)$ or $F(Z)$. (In the case illustrated the over-all shift parameter c is zero.)

So far no adjustable parameters have been introduced into the expression for ΔE (not counting the magic numbers M_i, which are considered as given). Three straightforward generalizations are possible which introduce two adjustable parameters but do not complicate essentially the form of the shell correction.

3.2. INCOMPLETE BUNCHING

If, instead of completely degenerate levels t_i, we consider partially bunched bands, the shell correction ΔE will be modified. Consider the case in which the width of each band is $(1-b)$ times its unbunched width, so that b may be regarded as a "bunching factor" – no bunching corresponding to $b = 0$ and complete bunching to $b = 1$. If the compression of the bands in fig. 3 is taken to be "uniform" in the sense that the position of each level in the energy spectrum varies linearly with b, it follows immediately that the energy difference ΔE is simply proportional to b. Thus the effect of partial bunching is to replace t_F in eq. (4) by bt_F, where b is the degree of bunching.

3.3. POTENTIAL ENERGY AND ITS VELOCITY DEPENDENCE

Eq. (4) was derived by considering the differences in kinetic energies for a gas of independent particles with a bunched and unbunched spectrum. For independent particles in an external potential well of constant depth the potential energy is the same for all particles and independent of the bunching, so that the inclusion of the potential energy would leave the energy difference ΔE unchanged. The situation is, however, more complicated, since it is necessary to have a velocity-dependent potential well if a self-consistent Fermi-gas description of a saturating system, like a nucleus, is attempted. (See, for example, the discussion in ref. [11]). (For a velocity-independent well the binding energy per particle cannot be made equal to the separation energy, and summing the energies of the individual particles in order to represent the total energy of such a system implies an internal inconsistency.) A velocity-dependent potential will affect our expression for ΔE since the modification of the kinetic energies implied by the bunching of the levels will also affect the depths felt by the particles and consequently modify the potential energy. The assumption of a general velocity dependence would complicate our expression for ΔE, but in the commonly used approximation in which the depth of the potential varies linearly with the kinetic energy of the particle, the modification in ΔE is, fortunately, trivial. Thus, if the well depth is taken as

$$v = v_0 + kt,$$

where v_0 and k are constants, and if the contribution of a particle to the total energy is taken as its kinetic energy t plus $(1/n)$ times the average potential v it experiences (n would be 2 for two-body forces), the total energy would be made up of contributions of the form

$$\varepsilon = \frac{v_0}{n} + \left(1 + \frac{k}{n}\right) t.$$

If now we assume the spectrum of the kinetic energies t to be bunched, the effect of the bunching will be $[1+(k/n)]$ times what it was in the case $k = 0$, corresponding to no velocity dependence. Hence the functional form of ΔE in eq. (4) is unaffected, the factor bt_F being simply replaced by $[1+(k/n)]bt_F$.

In what follows we shall lump the product of $[1+(k/n)]$, b and t_F into one adjustable parameter C (of the dimensions of energy).

3.4. PREDOMINANT SIGN OF ΔE

If, after putting the bunched levels t_i at the centre of gravity of the unbunched bands, the whole bunched spectrum is moved bodily down by a constant, we obtain a somewhat more general expression for the shell correction. It is still of the form of eq. (4) but the staircase function is now defined by the constants

$$\frac{3}{5}\frac{M_i^{\frac{5}{3}}-M_{i-1}^{\frac{5}{3}}}{M_i-M_{i-1}}-\frac{c}{2^{\frac{2}{3}}}, \qquad \text{for} \quad M_{i-1} < n < M_i,$$

where c is an adjustable over-all-shift parameter. (The factor $2^{\frac{2}{3}}$ is introduced for future notational convenience.) The freedom gained by the introduction of c makes it possible to vary the over-all behaviour of ΔE from a predominantly positive to a predominantly negative function. Contrary to what one might, perhaps, have expected, the choice $c = 0$ (bunched levels at average positions) does not result in a correction ΔE that is about equally often positive as negative, but in one that is entirely positive except at doubly magic numbers (N, Z both magic), at which it is zero. This becomes clear if one notes that for N and Z magic the total energy in the bunched case is made up of contributions from filled bands, each band being at what its average position was before the bunching; consequently the energy is, by definition, unaffected by the bunching. It is only the energy of an uncompleted band that will be affected and the effect of bunching will always be positive since the centre of gravity of an uncompleted band of levels is raised by bunching. The expression (4) for ΔE represents, therefore, a correction consisting entirely of positive bumps. The introduction of the parameter c allows one to lower the correction, making it sometimes positive and sometimes negative. The explicit dependence on N and Z of the modification introduced by c is readily seen to be equal to

$$\frac{1}{2^{\frac{2}{3}}}\,\frac{-\int_0^N c\,dn-\int_0^Z c\,dn}{(\frac{1}{2}A)^{\frac{2}{3}}};$$

i.e., equal to $-cA^{\frac{1}{3}}$.

As we shall see, the introduction of an over-all shift into the spectrum of levels is clearly demanded by the data. To date we have been unsuccessful in providing a theoretical justification for such a shift or in making an estimate from first principles of its magnitude. We feel that such an estimate ought to be possible from a careful

analysis of the behaviour of the centre of gravity of a group of levels, originally degenerate, when the degeneracy is removed by a deformation of the system.

The final form of the function $s(N, Z)$ arrived at in this section, is summarized below

$$s(N, Z) = \frac{F(N)+F(Z)}{(\frac{1}{2}A)^{\frac{2}{3}}} - cA^{\frac{1}{3}},$$

$$F(N) = \int_0^N [q(n) - n^{\frac{2}{3}}]\,\mathrm{d}n,$$

$$q(n) = \frac{3}{5}\frac{M_i^{\frac{5}{3}} - M_{i-1}^{\frac{5}{3}}}{M_i - M_{i-1}}, \qquad \text{for} \quad M_{i-1} < n < M_i. \tag{5}$$

We took the magic numbers as $M_i = 2, 8, 14$ (or 20), 28, 50, 82, 126, 184 for both neutrons and protons. The quantity M_0 is defined as zero. For purposes of illustration we also took $N = 258$ to be a magic number – see subsect. 7.8. We note that since $q(n)$ is a constant between M_{i-1} and M_i the dependence of $F(N)$ on N is of the form: (const)+(const)$N-\frac{3}{5}N^{\frac{5}{3}}$. Explicitly,

$$F(N) = q_i(N - M_{i-1}) - \tfrac{3}{5}(N^{\frac{5}{3}} - M_{i-1}^{\frac{5}{3}}), \qquad \text{for} \quad M_{i-1} < N < M_i.$$

At magic numbers $F(M_i)$ assumes the value zero. The appearance of $S(N, Z)$, equal to C times $s(N, Z)$, is illustrated in figs. 5 and 6. The first shows a contour plot of $S(N, Z)$; the second shows $S(N, Z)$ taken along a smooth line in the N, Z plane, following approximately the valley of β-stability, and given by Green's expression (ref. [1]), p. 250):

$$N - Z = \frac{0.4A^2}{A+200}.$$

4. The Deformability of Nuclei and the Attenuating Function

A detailed description of the shape-dependence of shell anomalies in the nuclear binding energy would be a most difficult task entailing the consideration of details of nuclear structure. Our choice of a simple short-range function (a Gaussian) for the description of the damping out of shell effects has been guided by qualitative considerations, supplemented by a model calculation (due to Hill and Wheeler) of non-interacting particles in a cubical box (ref. [14]), p. 1124).

The idea that there should be an attenuating function at all is, of course, the result of the observation that the known shell effects are associated with degeneracies characteristic of the spherical shape and should disappear with distortions away from the sphere. The basis of the whole of our treatment is that – apart from special configurations characterized by special symmetries – the nuclear deformation energy should follow a smooth, statistical, average behaviour (to which a liquid-drop

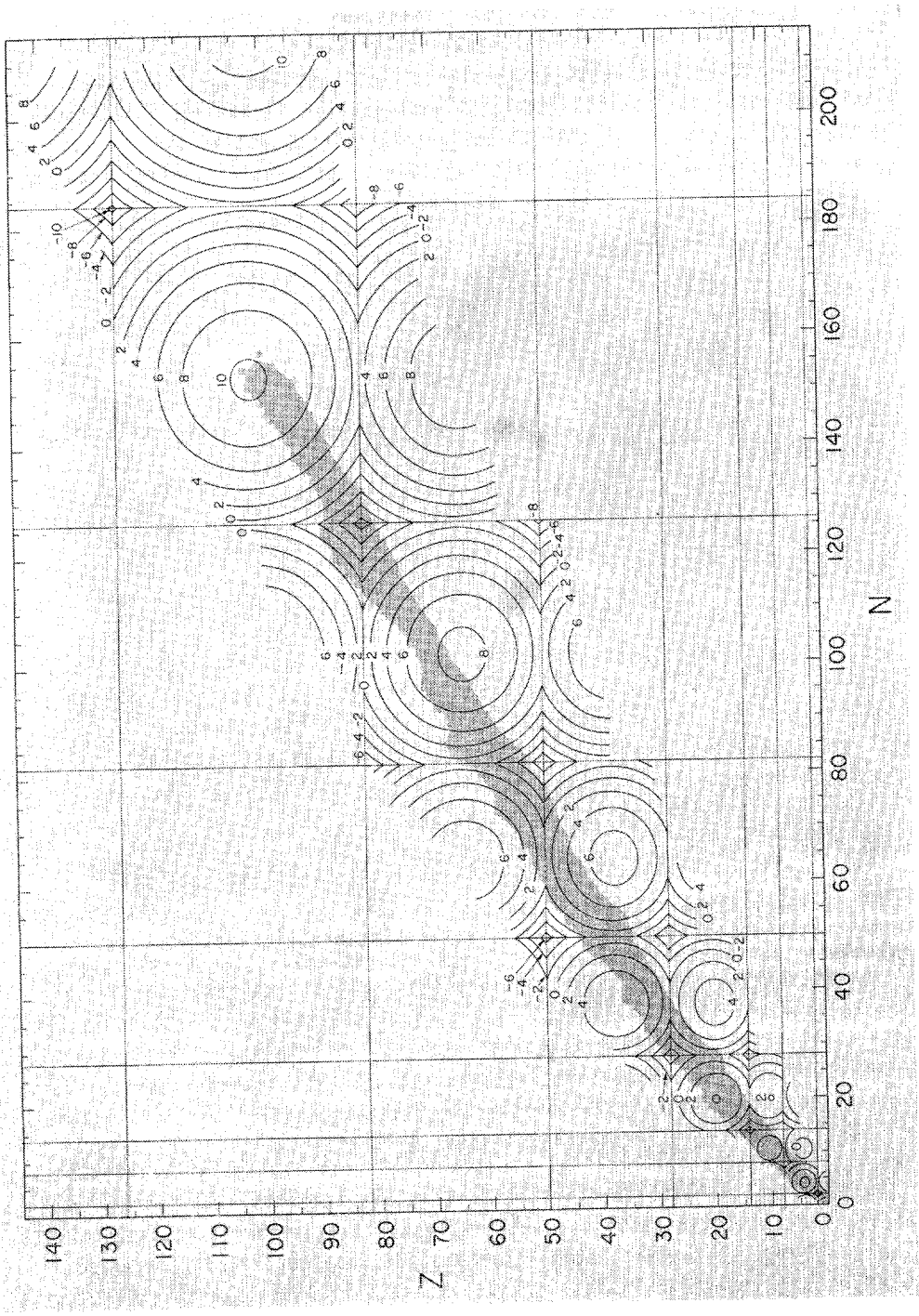

Fig. 5. The level lines, in MeV, of the two-dimensional shell function $S(N, Z)$ are shown. The gray band corresponds to the region of nuclei with measured masses. The doubly-magic combinations $N = 184$, $Z = 82$, 126 are hypothetical.

formula represents an adequate approximation). This concept of an average, amorphous state of a piece of irregularly shaped nuclear matter, characterized by an approximately constant volume density and a relatively thin surface region, provides the background for our discussion of nuclear deformabilities. Thus when attempting to trace out the energy of a nucleus as a function of deformation from a sphere we claim to be able to predict the average behaviour of the potential-energy curve as soon as the special degeneracies associated with the spherical shape have been broken down. This behaviour should be that of the amorphous, standard piece of nuclear matter, given by a suitable smooth (liquid-drop) formula. This requirement – a kind of correspondence principle – ought to provide a stabilizing factor in discussions of nuclear deformabilities. As soon as special degeneracies have been broken down, a smooth, familiar, predictable trend ought to set in.

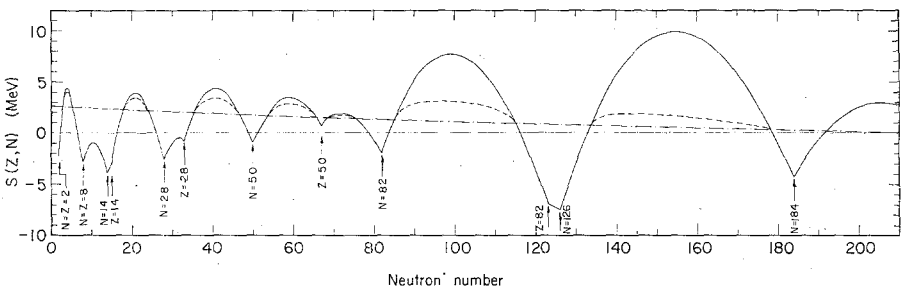

Fig. 6. The shell function $S(Z, N)$ is shown along Green's approximation to the valley of stability (solid line). The dot-and-dash line corresponds to the critical value S_{crit} which, when exceeded, leads to the appearance of deformations and a flattening-out of the humps in S, given by the dashed lines.

This "correspondence principle" for nuclear deformabilities – the existence of a definite asymptotic behaviour for larger deformations – appears not to have been exploited in existing discussions of nuclear deformabilities. The reason for this is probably that the majority of calculations of nuclear deformabilities have been made with the aid of a non-isotropic harmonic oscillator potential. This potential, although excellent for many purposes, is grossly inadequate in that it fails to represent a basic nuclear property, namely the saturating character of nuclear matter, i.e., the existence of an approximately constant nuclear density and a relatively thin nuclear surface. It is nuclear saturation that makes possible the division of a nucleus into a volume and surface region and the interpretation of average trends of nuclear masses in terms of a liquid-drop model. The oscillator nuclear potential, being all "surface", gives up from the beginning this basic aspect of nuclear structure. As a result, the possibility of establishing a connection between the deformabilities calculated on the basis of oscillator levels and the liquid-drop deformabilities is forfeited. We believe that any calculation of deformabilities based on the oscillator potential is subject to an arbitrariness which cannot be removed until the non-saturating character of this potential has been remedied.

Assuming the correctness of the notion of an asymptotic, average behaviour of a distorted nucleus, the qualitative characteristics of the shape dependence of a shell effect become, of necessity, that of a local (positive or negative) "dimple" in the potential-energy surface. The location of the dimple corresponds to the special configuration responsible for the shell effect, the most familiar such configuration being the sphere.

As regards the choice of the functional form of the dimple we have been guided by qualitative considerations. Since the shell effect should be destroyed by *any* deformation (e.g., a prolate or oblate quadrupole deformation, or a surface ripple of a higher multipole order) we have chosen for our deformation variable the root-mean-square of the deviation of the surface from a sphere, a quantity which incorporates indiscriminately all types of deformation. In fact the attenuation of a shell effect will surely depend in some specific way on the form of the deformation; in the absence of information on this dependence, our choice of the indiscriminate root-mean-square deviation may be regarded as an interim one, to be modified when future analysis brings out the need for a more refined treatment.

As regards the choice of a constant range in the attenuating function (a range independent of the nuclear size), we were guided by the expectation that the amount of distortion of a nuclear surface from a sphere required to destroy a shell effect would be of the order of magnitude of the Fermi wavelength $\lambda\!\!\!^{-}$ of the fastest particle in the nucleus. For a Fermi gas at a fixed density this length is a constant. The quantity $\lambda\!\!\!^{-}$ is a characteristic length, by means of which the Fermi gas can "feel out" deviations of the nuclear surface from a sphere, and we expect it to be a natural unit in which such deviations should be measured.

This argument can be made more precise by means of dimensional analysis. A nucleus is characterized by two quantities of the dimensions of a length, its radius R and the average spacing between nucleons (or the Fermi wavelength $\lambda\!\!\!^{-}$). Hence its energy as a function of a deformation magnitude ΔR (say the root-mean-square deviation considered above) should be expressible as

$$F\left(\frac{\Delta R}{\lambda\!\!\!^{-}}, \frac{\Delta R}{R}\right).$$

This is a function of *two* arguments. If, however, we consider the usual expansion in powers of $\lambda\!\!\!^{-}/R$, or $A^{-\frac{1}{3}}$, the above function may be written, to leading order, as a sum of two functions of one variable (see below)

$$F\left(\frac{\Delta R}{\lambda\!\!\!^{-}}, \frac{\Delta R}{R}\right) \to G\left(\frac{\Delta R}{\lambda\!\!\!^{-}}\right) + H\left(\frac{\Delta R}{R}\right).$$

The second term, independent of the microscopic quantity $\lambda\!\!\!^{-}$, may be identified as an over-all deformability (e.g., given by a surface energy). The first term, representing the deviation from this asymptotic behaviour, is the shell correction, whose charac-

teristic range is seen to be the constant $\lambda\!\!\!^{-}$. To prove the decomposition of F note that if $R/\lambda\!\!\!^{-}$ is sufficiently large it is possible to choose a deformation ΔR_1 such that $\Delta R_1/\lambda\!\!\!^{-} \gg 1$ but $\Delta R_1/R \ll 1$. It follows that

$$\text{for } \Delta R < \Delta R_1\text{: } F\left(\frac{\Delta R}{\lambda\!\!\!^{-}}, \frac{\Delta R}{R}\right) \to F\left(\frac{\Delta R}{\lambda\!\!\!^{-}}, 0\right),$$

$$\text{for } \Delta R > \Delta R_1\text{: } F\left(\frac{\Delta R}{\lambda\!\!\!^{-}}, \frac{\Delta R}{R}\right) \to F\left(\infty, \frac{\Delta R}{R}\right).$$

Assuming that the limits denoted by $F(\Delta R/\lambda\!\!\!^{-}, 0)$ and $F(\infty, \Delta R/R)$ as well as $F(\infty, 0)$ exist, we may readily verify that the combination

$$\Phi \equiv F\left(\frac{\Delta R}{\lambda\!\!\!^{-}}, 0\right) + F\left(\infty, \frac{\Delta R}{R}\right) - F(\infty, 0)$$

constitutes an approximation to the function $F(\Delta R/\lambda\!\!\!^{-}, \Delta R/R)$. Thus, evaluating the difference $\Phi - F$ in the two cases $\Delta R < \Delta R_1$ and $\Delta R > \Delta R_1$, we have

$$\text{for } \Delta R < \Delta R_1\text{: } \Phi - F = F\left(\frac{\Delta R}{\lambda\!\!\!^{-}}, 0\right) + F(\infty, 0) - F(\infty, 0) - F\left(\frac{\Delta R}{\lambda\!\!\!^{-}}, 0\right) = 0,$$

$$\text{for } \Delta R > \Delta R_1\text{: } \Phi - F = F(\infty, 0) + F\left(\infty, \frac{\Delta R}{R}\right) - F(\infty, 0) - F\left(\infty, \frac{\Delta R}{R}\right) = 0.$$

Hence the function Φ, a sum of a function of $\Delta R/\lambda\!\!\!^{-}$ and a function of $\Delta R/R$, is, under the conditions stated, an approximation to the function $F(\Delta R/\lambda\!\!\!^{-}, \Delta R/R)$.

The considerations of this section may be illustrated by a study of the deformability of a cubic box, containing a Fermi gas of independent particles. This example is due to Hill and Wheeler [14]) and we shall present a somewhat revised discussion of their results.

Fig. 7 shows a plot of the energy of a box, filled with 60 spinless particles, as a function of a deformation that stretches one side c and squeezes the other two a and b in a volume-preserving manner

$$a = L\mathrm{e}^{-\frac{1}{2}\alpha}, \qquad b = L\mathrm{e}^{-\frac{1}{2}\alpha}, \qquad c = L\mathrm{e}^{\alpha}.$$

The potential is constant inside the box and infinite outside, so that the wave functions of the particles are sines and cosines and the total energy is given by a sum of squares of positive integers l, m, n

$$E = \frac{\hbar^2\pi^2}{2ML^2} \sum_{l,m,n}' \left[\frac{l^2}{\mathrm{e}^{-\alpha}} + \frac{m^2}{\mathrm{e}^{-\alpha}} + \frac{n^2}{\mathrm{e}^{2\alpha}}\right]$$

(M is the particle mass). Each of the parabola-like curves in fig. 7 shows the behaviour of the energy for a given choice of "orbitals" (a given assignment of the quantum

numbers l, m, n) for the 60 particles. The scalloped envelope of the parabolas would then be the lowest deformation energy corresponding to allowing the particles to re-adjust themselves to the lowest possible orbitals for each deformation. The dashed curve represents the trend of the deformability calculated in the average, amorphous,

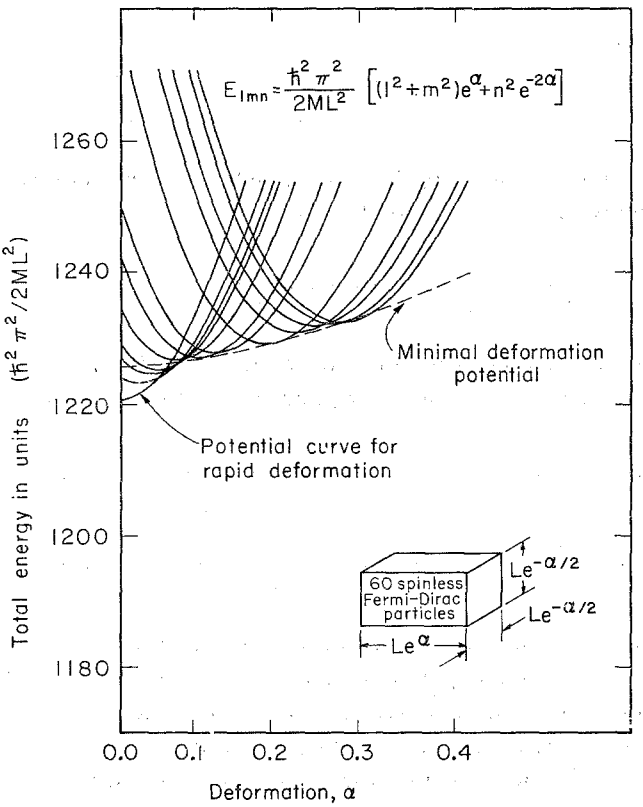

Fig. 7. A plot of the deformation energy of 60 particles in a rectangular box of volume L^3, as a function of a deformation parameter α. The parabola-like curves correspond to keeping the single-particle orbitals fixed; their envelope builds up a scalloped curve corresponding to a minimal deformation potential, which is compared with a statistical calculation (dashed curve).

statistical approximation carried out to an order in $A^{-\frac{1}{3}}$ in which volume and surface energies are retained. Only the curvature of the dashed curve is significant – the absolute position has been adjusted to facilitate comparison with the scalloped curve. (To calculate the absolute position of the dashed curve, terms of higher order in $A^{-\frac{1}{3}}$ would have to be retained.)

The equation of the dashed curve may be deduced from the second term in Hill and Wheeler's equation appearing at the top of p. 1125 of ref. [14]). The above authors identify this term with a surface energy which they write in the form $(S/32\pi)(6\pi^2N/V)^{\frac{4}{3}}$, N being the number of particles in the box, V the volume and S the surface area.

Hill and Wheeler, in constructing their fig. 12 (on which our fig. 7 is based), take the volume of the box to be π^3 so that its surface is $S = 2\pi^2 e^{-\alpha} + 4\pi^2 e^{\frac{1}{2}\alpha}$. Hence, with $N = 60$, they find for the surface energy (ref. [14]), p. 1125, caption to fig. 12):

$$\frac{\pi}{16}\left(\frac{360}{\pi}\right)^{\frac{2}{3}}(e^{-\alpha}+2e^{\frac{1}{2}\alpha}) = \frac{\pi}{16}\left(\frac{360}{\pi}\right)^{\frac{2}{3}}(3+\tfrac{3}{4}\alpha^2 \ldots)$$

$$= 328+82\alpha^2, \text{ approximately.}$$

This is the expression on which our dashed curve is based (apart from an arbitrary shift upward). Hill and Wheeler's dashed curve labelled "Predicted by Surface Tension Argument" disagrees with our dashed curve for a reason that we do not understand; we have used Hill and Wheeler's own expression for what they call the surface energy.

Concerning the separate question whether this expression should be identified with a surface energy we would refer to ref. [31]), especially the discussion in sect. 5. The essence of that discussion is that for a Fermi gas of particles in a box with infinitely high walls the particle density is confined effectively to a somewhat smaller box whose surface is at a distance $\frac{1}{8}(3\pi)\lambda\!\!\!^{-}$ inside the potential box ($\lambda\!\!\!^{-}$ is the wavelength of the fastest particle in the gas). It then follows that if the volume of the outer box is kept constant with deformation the volume of the inner one is not quite constant; it decreases by an amount proportional to the increase of the surface area. As a result the density of the Fermi gas increases slightly and, since the kinetic energy by itself is not stationary with respect to density changes, the volume energy of the system increases. This compression being proportional to the increase in surface area, the associated energy change is also proportional to the change in area and thus makes a spurious contribution to the true surface energy. In the case of a box with infinite walls these contributions can all be calculated explicitly, with the result that of the expression identified by Hill and Wheeler as a surface energy, *four-fifths* arises from the compression of the system and one-fifth from the true surface energy.

[The surface energy of a Fermi gas characterized by a Fermi energy t_F and enclosed in a box with infinitely steep sides may be deduced from ref. [31]) and re-written in the form

$$4\pi r_0^2 \gamma = \frac{3\pi}{40}\left(\frac{3}{\pi}\right)^{\frac{1}{3}} t_F,$$

where $\frac{4}{3}\pi r_0^3$ is the volume per particle and γ the surface energy per unit area. The energy due to the compression of the box, if expressed – incorrectly – as a contribution to the surface energy is found to be

$$4\pi r_0^2 \gamma_{\text{spurious}} = \frac{3\pi}{10}\left(\frac{3}{\pi}\right)^{\frac{1}{3}} t_F.$$

The sum of the two expressions leads to a value of $(\gamma+\gamma_{\text{spurious}})$ which agrees with the quantity that Hill and Wheeler denote by O_{kin} on p. 1125, ref. [14]). The ratio $\gamma/(\gamma+\gamma_{\text{spurious}})$ was given in ref. [31]), p. 235, as 0.194. The correct value is $\frac{1}{5}$ exactly].

The fact that a slight compression of a system whose energy is not stationary with respect to density changes may introduce large spurious contributions to the surface energy is very important for the correct interpretation of calculations dealing with the deformability of single-particle systems. It does not invalidate, however, the illustrative value of Hill and Wheeler's box, which shows the relation of single-particle calculations to the deformability obtained in the amorphous, statistical approximation, provided both calculations are made under the *same* conditions. Thus our fig. 7 shows this relation when both calculations are made for a box of constant volume (and so four-fifths of the rise of the dashed curve is due to compression and one-fifth to surface tension).

With this understanding we may still conclude that the amorphous, asymptotic deformability represents rather well the trend of the single-particle calculation, except for a sizable deviation near the cubical shape $\alpha = 0$. The reason for this deviation is itself instructive. It turns out that 60 happens to be a magic number for particles in a cubic box, and the special stability of the cubical shape in fig. 7 is a reflection of this shell effect. We can thus see in fig. 7 not only how the amorphous deformability reproduces the single-particle calculations, but also how the special stability of a closed shell is destroyed by a deformation. In the case illustrated in fig. 7, at least, the representation of the shell effect by a Gaussian function of distortion would appear not to be misleading. We may even verify that the range of the negative bump in fig. 7 is of the order of magnitude of the range of our Gaussian attenuating function. Thus we readily calculate that the mean-square deviation of the surface of a box from the cube is given by $\frac{1}{8}L^2\alpha^2$ (for small α). With four particles per state (neutrons and protons with two spin directions) the box with 60 filled orbitals corresponds to a nucleus with 240 particles, and hence the volume per particle is given by $\frac{1}{240}L_0^3$, equal to $\frac{4}{3}\pi r_0^3$, say. Using this relation between L and r_0 we may rewrite the mean-square deviation as $\frac{1}{2}(40\pi)^{\frac{2}{3}} r_0^2\alpha^2$. Imagining the bump in fig. 7 to be represented by a Gaussian and estimating by eye that its amplitude is halved at $\alpha = 0.04$ or 0.05, we find for the range a of the Gaussian the relation

$$\frac{a}{r_0} \approx \frac{(0.04 \text{ or } 0.05)(40\pi)^{\frac{1}{3}}}{2^{\frac{1}{2}} \ln 2} = (0.17 \text{ or } 0.26),$$

which is to be compared with $a/r_0 = 0.27$, for the attenuating function in our mass formula (see sect. 6).

There are now available more refined calculations [2-4]) which study the deformability of nuclei by starting with single-particle levels in an oscillator potential and consider the effect of residual interactions between the particles. The effect of these interactions is to smooth out the scallops in fig. 7 and the result, as regards the

damping-out of shell effects, appears to improve the correspondence with a smooth attenuation function superimposed on an asymptotic trend of the deformation energy.

5. The Mass Formula

Assuming the shell function from sect. 3 and a Gaussian attenuating function (sect. 4), the shell correction M_{shells} is now completely defined through eqs. (1) and (5). It contains three adjustable parameters: the amplitude parameter C, the shift or base-line parameter c and the range parameter a. In this section we shall combine the shell correction with a four-parameter liquid-drop formula to obtain

$$M(N, Z, \text{shape}) = M_{\text{n}}N + M_{\text{H}}Z + (\text{volume energy}) + (\text{surface energy}) + (\text{Coulomb energy}) + \delta + S(N, Z)\exp[-\overline{(\delta R)^2}/a^2]. \quad (6)$$

In the above, M_{n} is the neutron mass and M_{H} the mass of the hydrogen atom. Further, we shall take

$$\text{volume energy} = -c_1 A,$$
$$\text{surface energy} = c_2 A^{\frac{2}{3}} f(\text{shape}).$$

Here c_1 is the volume binding energy per particle, whose dependence on nuclear composition will be taken as

$$c_1 = a_1 \left[1 - \kappa \left(\frac{N-Z}{A}\right)^2\right],$$

where a_1 and κ are constants. The surface-energy coefficient c_2, equal to $4\pi r_0^2$ times the nuclear surface energy per unit area, will be taken to depend on nuclear composition in the same way as c_1

$$c_2 = a_2 \left[1 - \kappa \left(\frac{N-Z}{A}\right)^2\right].$$

We adopt this form for the surface energy not because we can discern any evidence for it in the nuclear masses, but because the expression

$$(a_1 A - a_2 A^{\frac{2}{3}}) \left[1 - \kappa \left(\frac{N-Z}{A}\right)^2\right]$$

is an intrinsically more reasonable three-parameter binding-energy formula, in which the surface and volume energies vary in a parallel manner and, in particular, vanish simultaneously for a large neutron excess. (Conventional formulae without a composition-dependent surface energy correspond to a surface tension that retains its full standard value even when the neutron excess has made the volume binding vanish, and all cohesion has been lost.)

The second minor modification that we shall adopt will be that instead of the formula

$$\frac{3}{5}\frac{e^2}{r_0}\frac{Z^2}{A^{\frac{1}{3}}}g(\text{shape})$$

for the electrostatic energy, we shall take the following expression:

$$\text{electrostatic energy} = \frac{3}{5}\frac{e^2}{r_0}\frac{Z^2}{A^{\frac{1}{3}}}g(\text{shape}) - \frac{\pi^2}{2}\frac{e^2}{r_0}\left(\frac{d}{r_0}\right)^2\frac{Z^2}{A}.$$

As will be shown in appendix A.2, the second term corrects the electrostatic energy of an *arbitrarily shaped* drop for a diffuseness of the charge distribution. The correction is to lowest order in the surface-thickness parameter d in a Fermi (Woods-Saxon) type of distribution specifying the fall-off of the charge density across the surface of the drop. According to the Stanford electron-scattering experiments d is given by $(2.4)/(2\ln 9) = 0.5461$ fm.

The above modification in the electrostatic energy is again not made on account of any evidence from the nuclear masses but because it incorporates a well-established property of nuclei without introducing additional parameters and without complicating appreciably the mass equation.

The term δ in eq. (6) is an even-odd correction, which we shall take as $\pm 11/A^{\frac{1}{2}}$ MeV for odd or even nuclei and zero for odd-mass nuclei [12]).

The function f (shape) gives the dependence of the surface energy on shape and is equal to the dimensionless ratio of the surface area of the shape in question to the area of the original sphere. The function g (shape) is the dimensionless ratio of the electrostatic energy of a distorted sharp distribution to that of the sphere.

The shape dependence of the mass in eq. (6) comes in through the liquid-drop functions f (shape) and g (shape) and through the attenuating factor $\exp[-\overline{(\delta R)^2}/a^2]$. If we choose to describe the shape of the nucleus by

$$R(\theta, \phi) = R_0[1 + \sum_\lambda \sum_\mu a_{\lambda\mu} Y_{\lambda\mu}(\theta, \phi)],$$

we find

$$\overline{(\delta R)^2} = \frac{R_0^2}{4\pi}\beta^2$$

where

$$\beta^2 = \sum_\lambda \sum_\mu |a_{\lambda\mu}|^2, \tag{7}$$

$$f = 1 + \sum_\lambda \frac{(\lambda-1)(\lambda+2)}{8\pi}|a_{\lambda\mu}|^2 + \text{higher powers of } a_{\lambda\mu},$$

$$g = 1 - \sum_\lambda \frac{5(\lambda-1)}{4\pi(2\lambda+1)}|a_{\lambda\mu}|^2 + \text{higher powers of } a_{\lambda\mu}.$$

In the case of an axially symmetric shape, described by

$$R(\theta) = R_0[1+\sum_n a_n P_n(\cos\theta)], \tag{8}$$

we have

$$\overline{(\delta R)^2} = R_0^2 \sum_n \frac{a_n^2}{2n+1},$$

$$f = 1+\sum_n \frac{(n-1)(n+2)}{2(2n+1)} a_n^2 + \ldots,$$

$$g = 1-\sum_n \frac{5(n-1)}{(2n+1)^2} a_n^2 + \ldots.$$

The higher powers in these expansions may be found in refs. [9,13]). In particular, if only a_2 is retained, we have

$$\overline{(\delta R)^2} = R_0^2 \tfrac{1}{5} a_2^2,$$
$$f = 1+\tfrac{2}{5}a_2^2 - \tfrac{4}{105}a_2^3 + \ldots,$$
$$g = 1-\tfrac{1}{5}a_2^2 - \tfrac{4}{105}a_2^3 + \ldots.$$

In the case of an ellipsoidal shape described with the aid of a deformation parameter σ and a shape parameter γ, related to the semi-axes a, b, c by

$$a = R_0 \exp[\sigma\cos(\gamma-\tfrac{2}{3}\pi)],$$
$$b = R_0 \exp[\sigma\cos(\gamma+\tfrac{2}{3}\pi)],$$
$$c = R_0 \exp[\sigma\cos\gamma],$$

we find, using ref. [15]),

$$\overline{(\delta R)^2} = R_0^2 \tfrac{1}{5}\sigma^2(1-\tfrac{1}{7}\sigma\cos 3\gamma) + \text{higher powers of } \sigma,$$
$$f = 1+\tfrac{2}{5}\sigma^2 - \tfrac{2}{21}\sigma^3\cos 3\gamma + \text{higher powers of } \sigma,$$
$$g = 1-\tfrac{1}{5}\sigma^2 - \tfrac{1}{105}\sigma^3\cos 3\gamma + \text{higher powers of } \sigma.$$

Because our definition of $\overline{(\delta R)^2}$ is more directly related to β^2 than to σ^2, it is convenient for our purposes to retain β^2 (or rather a multiple thereof) as a deformation variable in place of σ^2 even for ellipsoidal distortions. According to ref. [15]) the relation between σ^2 and β^2 is

$$\beta^2 = \tfrac{4}{5}\pi\sigma^2(1-\tfrac{1}{7}\sigma\cos 3\gamma + \text{higher powers of } \sigma)$$

and if we introduce $(5/4\pi)\beta^2$ as our variable, denoted by α^2, we may write the last set of equations for $\overline{(\delta R)^2}$, f, and g as

$$\overline{(\delta R)^2} = R_0^2 \tfrac{1}{5}\alpha^2,$$
$$f = 1+\tfrac{2}{5}\alpha^2 - \tfrac{4}{105}\alpha^3\cos 3\gamma + \text{higher powers of } \alpha,$$
$$g = 1-\tfrac{1}{5}\alpha^2 - \tfrac{4}{105}\alpha^3\cos 3\gamma + \text{higher powers of } \alpha.$$

The deformation magnitude α, proportional to the root-mean-square deviation of the surface from a sphere, is to first order equal to σ, and for axially symmetric shapes described by eq. (8) is identical with a_2. The explicit form of our mass equation for small ellipsoidal deformations is thus

$$M(N, Z; \alpha, \gamma) = M_n N + M_H Z - c_1 A + c_2 A^{\frac{2}{3}}(1 + \tfrac{2}{5}\alpha^2 - \tfrac{4}{105}\alpha^3 \cos 3\gamma) + c_3 \frac{Z^2}{A^{\frac{1}{3}}}(1 - \tfrac{1}{5}\alpha^2 - \tfrac{4}{105}\alpha^3 \cos 3\gamma) - c_4 \frac{Z^2}{A} + S(N, Z) \exp(-\alpha^2/\alpha_0^2) + \delta, \tag{9}$$

where

$$c_3 = \frac{3}{5}\frac{e^2}{r_0},$$

$$c_4 = \frac{\pi^2}{2}\left(\frac{d}{r_0}\right)^2 \frac{e^2}{r_0},$$

$$\alpha_0^2 = 5a^2/R_0^2 = 5(a/r_0)^2 A^{-\frac{2}{3}}.$$

In order to display more clearly the dependence of the mass on deformation we introduce the deformation magnitude θ, defined as α/α_0, and re-write eq. (9) in the form

$$M = M_0 + E\theta^2 - F\theta^3 \cos 3\gamma + S e^{-\theta^2}, \tag{10}$$

where

$$M_0 = M_n N + M_H Z - c_1 A + c_2 A^{\frac{2}{3}} + c_3 \frac{Z^2}{A^{\frac{1}{3}}} - c_4 \frac{Z^2}{A} + \delta,$$

$$E = \left(\tfrac{2}{5}c_2 A^{\frac{2}{3}} - \tfrac{1}{5}c_3 \frac{Z^2}{A^{\frac{1}{3}}}\right)\alpha_0^2 = \tfrac{2}{5}c_2 A^{\frac{2}{3}}(1 - x)\alpha_0^2,$$

$$F = \tfrac{4}{105}\left(c_2 A^{\frac{2}{3}} + c_3 \frac{Z^2}{A^{\frac{1}{3}}}\right)\alpha_0^3 = \tfrac{4}{105}c_2 A^{\frac{2}{3}}(1 + 2x)\alpha_0^3.$$

In the above, M_0 is the mass of an undistorted liquid drop, E a coefficient specifying the stiffness of the liquid drop against small spheroidal distortions (and hence related in a simple way to the fissility parameter x, defined as the Coulomb energy term $c_3 Z^2/A^{\frac{1}{3}}$ divided by twice the surface energy $c_2 A^{\frac{2}{3}}$ – see appendix A.2). The coefficient F specifies the cubic term in the liquid-drop formula (through which also the γ-dependence enters).

As noted in sect. 2 the mass formula (10) will predict spherical equillibrium shapes if S is negative, but the stability of the sphere may be lost if S becomes sufficiently positive. The explicit discussion of the resulting equilibrium shapes and masses is particularly simple if the cubic term in F is disregarded. This is a fairly good ap-

proximation for nuclei throughout the periodic table (except for distortions so large that fission comes into consideration). We shall neglect for the moment the cubic term; the full eq. (10) is discussed in appendix A.1.

The condition for the instability of the sphere, and for the appearance of non-spherical equilibrium shapes is

$$\left.\frac{\partial^2 M}{\partial \theta^2}\right|_{\theta=0} < 0.$$

On carrying out the differentiation this condition may be written in the form $S > S_{\text{crit}}$, where S_{crit} is simply given by E, the coefficient of the quadratic term in eq. (10). Explicitly we have

$$S_{\text{crit}} = 2c_2(a/r_0)^2(1-x).$$

The quantity S_{crit} is a smooth function of N and Z (very nearly a straight line in a plot against x). In regions of the periodic table where the bumps in the shell function $S(N, Z)$ exceed this smooth function, deformed equilibrium shapes will appear.

The equilibrium configurations are defined by the conditions $\partial M/\partial\theta = 0$ and $\partial M/\partial\gamma = 0$. The second equation is always satisfied by $\gamma = 0$, $\pm\frac{1}{3}\pi$, or $\pm\frac{2}{3}\pi$. With the choice of $\gamma = 0$ the first equation becomes

$$E\theta - \tfrac{3}{2}F\theta^2 - S\theta e^{-\theta^2} = 0, \tag{11}$$

or

$$E\theta - S\theta e^{-\theta^2} = 0, \tag{12}$$

if F is neglected. Eq. (12) is satisfied either by $\theta = 0$ (the spherical configuration) or by

$$\theta = \pm[\ln (S/S_{\text{crit}})]^{\frac{1}{2}}. \tag{13}$$

This equilibrium deformation θ is thus a very slowly varying function of S/S_{crit}, except when S is close to S_{crit}, in which case θ becomes proportional to $\pm(S-S_{\text{crit}})^{\frac{1}{2}}$, a result anticipated in sect. 2.

In the quadratic approximation the mass of a stably deformed nucleus is found by substituting eq. (13) in eq. (10), with the F term omitted. The result is

$$M = M_0 + S_{\text{crit}} + S_{\text{crit}} \ln (S/S_{\text{crit}}). \tag{14}$$

Thus the original shell correction for a spherical nucleus, in the form of a bumpy function $S(N, Z)$, is replaced, for nuclei with stable deformations, by the flat function $S_{\text{crit}}(N, Z)$, augmented by the almost-flat function $S_{\text{crit}}\ln(S/S_{\text{crit}})$. The net effect is the flattening-out of those parts of the bumps in $S(N, Z)$ that exceed the quantity S_{crit}, the flattening-out being to a level somewhat in excess of this smooth function of N and Z (see fig. 6).

The two solutions corresponding to the + and − signs in eq. (13) correspond to

prolate and oblate shapes, respectively. In the quadratic approximation they have identical energies. The effect of the cubic term in eq. (10) is to lower the energy of the prolate shape with respect to the oblate shape. We may study this quantitatively by writing the equilibrium deformation as

$$\theta = \theta_0 + (\theta - \theta_0),$$

where θ_0 denotes the equilibrium deformation obtained in the quadratic approximation {i.e., $\theta_0 = \pm[\ln(S/S_{\text{crit}})]^{\frac{1}{2}}$} and $\theta - \theta_0$ is a small correction of order F/E. Solving the condition $\partial M/\partial\theta = 0$ to lowest order in F/E now gives (apart from certain subtleties discussed in appendix 1)

$$\theta = \theta_0 + \tfrac{3}{4}F/E$$

Thus the two deformations corresponding to $\theta_0 = \pm[\ln(S/S_{\text{crit}})]^{\frac{1}{2}}$ are both shifted towards positive values by the amount $\frac{3}{4}F/E$, which in practice amounts to a change of some 10 % at most. The energy of the equilibrium shapes perturbed by the presence of the cubic term turns out to be given, to first order in F/E, by

$$M_{\text{perturbed}} = M_{\text{unperturbed}}[\text{i.e., eq. (14)}] - F\theta_0^3 .$$

Thus the energy of the prolate shape $\{\theta_0 = +[\ln(S/S_{\text{crit}})]^{\frac{1}{2}}\}$ is decreased and the energy of the oblate shape $\{\theta_0 = -[\ln(S/S_{\text{crit}})]^{\frac{1}{2}}\}$ is increased, the energy changes involved being, in the present approximation, simply the values of the cubic term in the liquid-drop part of the mass formula, evaluated at the unperturbed equilibrium positions. The result is that the *prolate* shape is the truly stable configuration of equilibrium predicted by eq. (10). The oblate shape is unstable with respect to conversion into the prolate shape, the instability being associated, it turns out, with non-axially symmetric deformations described by γ. This may be verified from eq. (9) and is illustrated in fig. 8.

In addition to the two solutions discussed above, the condition $\partial M/\partial\theta = 0$ has, in general, a further solution. Thus, provided S is not too large, the last term in eq. (11) will become negligible for some sufficiently large value of θ, and eq. (11) may be satisfied approximately by

$$\theta = \tfrac{2}{3}E/F,$$

which, when re-written, states that

$$\alpha = \frac{7(1-x)}{1+2x}. \tag{15}$$

This is the well-known result for the equilibrium configuration corresponding to the saddle-point for the fission of a liquid drop, calculated in the cubic approximation, and with shell effects neglected. [The more familiar form of this result is obtained by considering x to be close to 1, when α becomes $\frac{7}{3}(1-x)$.]

The more complicated situation when all terms in eq. (11) are comparable at the saddle-point requires numerical solution of that equation.

In order to be able to describe saddle-point shapes in practice, it is usually essential to allow for more general deformations than the ellipsoidal deformation to which eq. (9) has been specialized. (Except when x is quite close to 1, e.g., $x \gtrsim 0.9$.

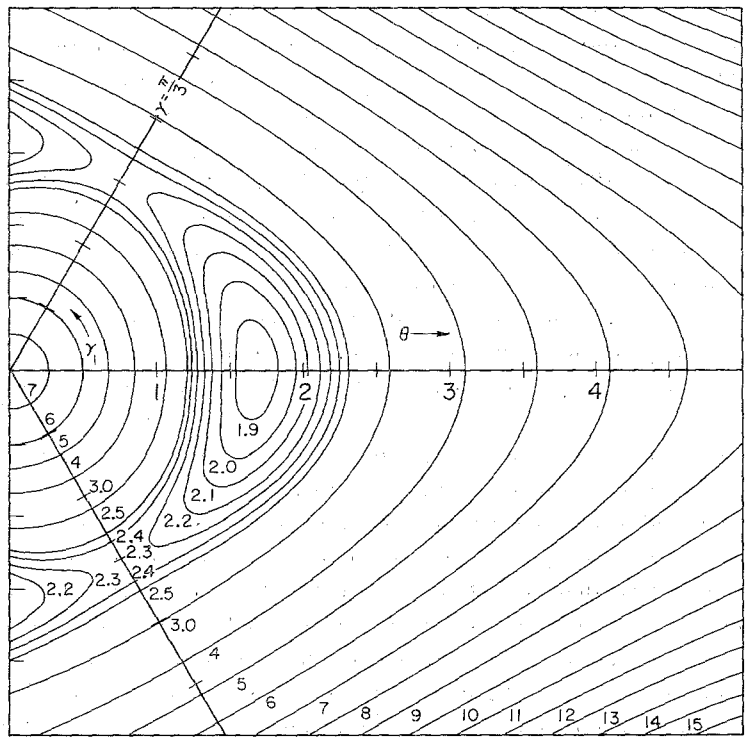

Fig. 8. An illustration of the θ and γ dependence of our mass formula for the case of ^{236}U. The level lines of the quantity $E\theta^2 - F\theta^3 \cos 3\gamma + S \exp(-\theta^2)$ are shown in MeV. Note the stable prolate shape at $\theta \approx 1.7$, $\gamma = 0$ and the unstable oblate shape at $\theta \approx 1.5$, $\gamma = \frac{1}{3}\pi$ (a saddle-point). The saddle-point for fission is beyond the range of the figure, on the extreme right.

when ellipsoids *are* adequate.) On the other hand, for the large distortions associated with saddle-point shapes for $x \lesssim 0.9$ our shell correction $Se^{-\theta^2}$ is essentially damped out and the determination of these saddle-point shapes may be taken over without modification from the existing calculations for the idealized liquid drop without shell effects [7]. We have indeed found it possible to include in our discussion the calculation of saddle-point masses – or fission barriers – for all nuclei in the periodic table (for details see subsect. 7.7. and appendix A.1).

6. Fitting of Adjustable Parameters

The data to be fitted by our mass formula (9) consist of the trends in about 1200 experimental ground-state masses and the trends in some 240 quadrupole moments. In addition, the experimental masses of some 40 heavy nuclei, not in their stable equilibrium configurations but in distorted, unstable "saddle-point" configurations, are also known experimentally or can be estimated from spontaneous fission half-lives. Insofar as our mass formula is supposed to describe distorted nuclei, these saddle-point masses should be included in a comparison of the formula with experiment. Although such nuclei are relatively few in number they are important in fixing certain of the parameters in the formula that are otherwise not very well determined (in particular the ratio of the electrostatic energy to the surface energy).

The mass formula (9) contains seven adjustable parameters, four in the liquid-drop part (a_1, a_2, c_3 and κ) and three in the shell correction (C, a and c). The problem of determining the seven parameters in a reasonably perspicuous way is not as difficult as it might seem, because the liquid-drop parameters govern the overall trends and the shell-correction parameters govern local irregularities, with the result that one may fit four of the parameters almost independently of the remaining three, allowing for the slight inter-dependence of the two determinations by a few iterations.

The first determination of the shell parameters C, a and c was made by using for the liquid-drop part of the formula the standard expression given by Green (ref. [1]), p. 287). This liquid-drop mass was subtracted from the experimental masses and a plot of the type given in fig. 21(a) was prepared. From the amplitude of the shell oscillation it was clear that the parameter C had to be in the neighbourhood of 5 or 6 MeV. A little experimentation with the values of a and c showed that the incidence of the nuclear deformations in the region of the rare earths and actinides on the one hand, and the magnitude of the deformations on the other, required this pair of numbers to be in the neighbourhood of $c \approx 0.27$ and $a/r_0 \approx 0.33$. These preliminary results are described in ref. [16]). Since that time we have developed a more systematic method of determining all the adjustable parameters. This method not only gives the values of the parameters rather directly, but also provides in most cases an objective test for the correctness of the *functional form* of the expressions assumed for the representation of the liquid-drop and shell-correction effects. The essence of the method is the usual artifice of plotting such combinations of the experimental data against such combinations of the arguments (e.g., N and Z) that, if the functional form of the mass formula were correct, a *straight line or a set of straight lines* would be obtained. The slopes and intercepts of the lines then give the values of the parameters sought, but, what is equally important, the conformation of the experimental points to linear trends tests the suitability of the functional form assumed. In practice the following procedures were followed.

6.1. DETERMINATION OF LIQUID-DROP PARAMETERS

Assume that approximate values of all the parameters have been obtained as explained above. The first step was then to subtract from the experimental masses the calculated shell correction, the calculated electrostatic energy and the even-odd correction δ (regarded as not subject to any significant uncertainty.) After further subtracting the nucleon masses $M_{\mathrm{n}}N+M_{\mathrm{H}}Z$ we are left with "corrected" experimental masses (or binding energies). The result so obtained, after division by the mass number A, should be equal to the specifically nuclear binding energy per particle, say Y. According to eq. (9) this quantity should have the form

$$Y = -(a_1 - a_2 A^{-\frac{1}{3}})\left[1-\kappa\left(\frac{N-Z}{A}\right)^2\right],$$

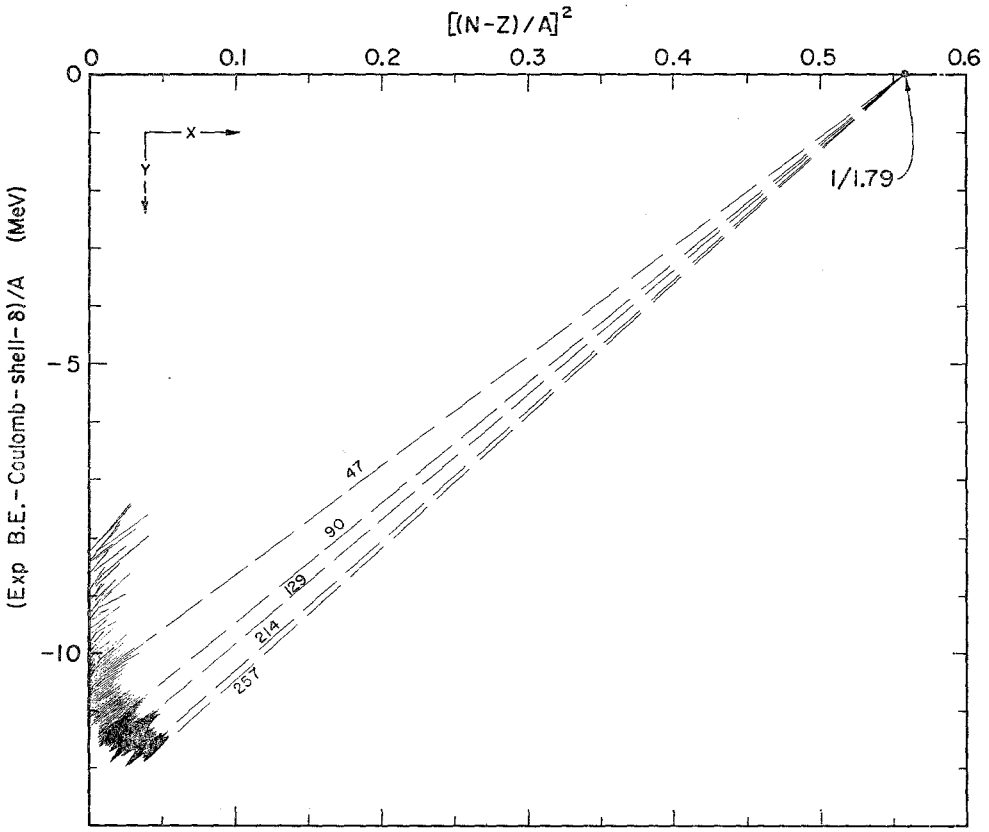

Fig. 9. The specifically nuclear binding energy per particle (corrected for shell effects), plotted as a function of the square of the relative neutron excess. The liquid-drop formula for nuclear masses predicts the result to be a series of straight lines, one for each A, the lines intersecting at a common point on the X-axis (shown as 1/1.79). Note the large distance from the region of the experimental data to this point. The labels on the dashed lines refer to A values. The intersections on the Y-axis should give a straight line when plotted as a function of $A^{-\frac{1}{3}}$. In this figure, as well as figs. 10–13, the adjustable parameters in the mass formula have the final values arrived at in sect. 6.

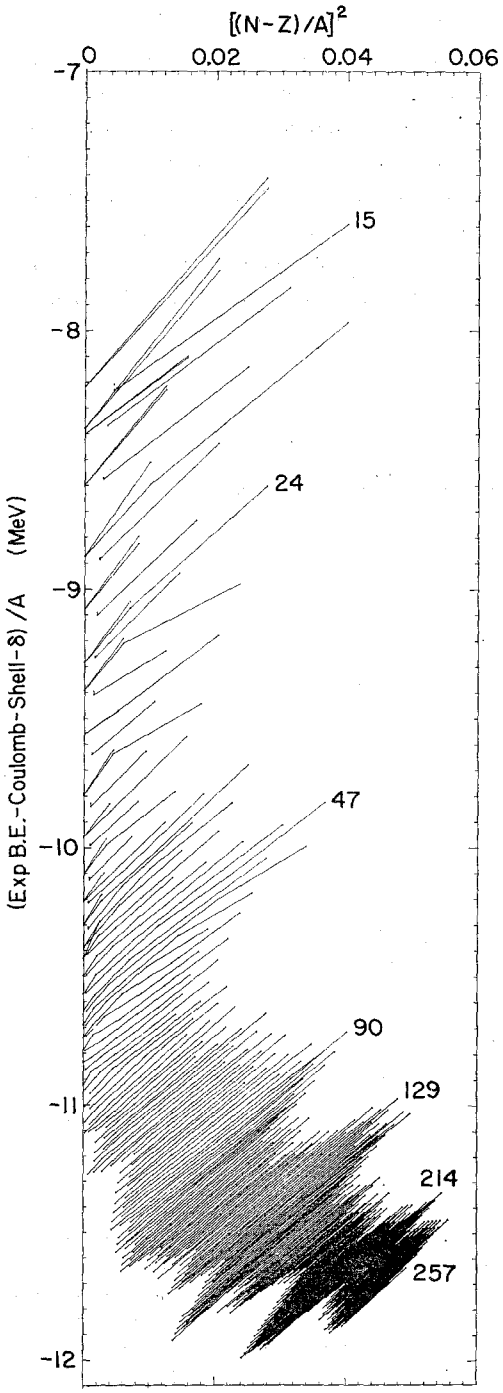

Fig. 10. A larger-scale version of fig. 9. (The original plot from which this figure was made was 1.3 m long, so that details in the heavy-element region could be resolved.) Note the "sagging" of the lines close to the ordinate axis, associated with the extra binding attributed to the Wigner term.

a function linear in $A^{-\frac{1}{3}}$ and in $[(N-Z)/A]^2$. This functional dependence is the essence of the liquid-drop assumption concerning the nuclear part of the binding energy. It can be tested by plotting the experimental values of Y against $[(N-Z)/A]^2$, which should result in a set of straight lines, one for each A. (This would hold even if $a_1-a_2A^{-\frac{1}{3}}$ were replaced by a general function of A.) All the lines, when extrapolated, should intersect the $Y = 0$ axis at the common point $[(N-Z)/A]^2 = 1/\kappa$,

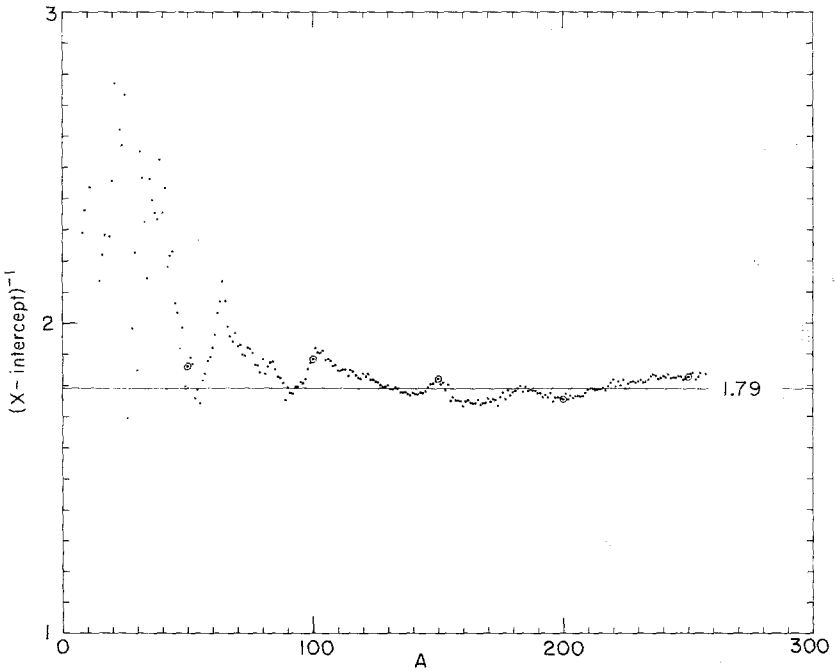

Fig. 11. The reciprocals of the X-intercepts from fig. 9 are plotted as a function of A and compared with the assumed constant value $\kappa = 1.79$. The circled points mark values of A equal to 50, 100, 150, 200 and 250. (Note the false zero on the ordinate axis.) Most of the deviations in the region of the lighter elements are positive – evidence once more of the Wigner term.

defining the parameter κ. On the other hand, the intercepts on the $[(N-Z)/A]^2 = 0$ axis give $-(a_1-a_2A^{-\frac{1}{3}})$ and these intercepts should, in turn, give a straight line when plotted against $A^{-\frac{1}{3}}$. The slope and intercept of this line define the parameters a_1 and a_2. Such plots are illustrated in figs. 9–12. (See also the next section.)

After a set of new specifically nuclear liquid-drop parameters a_1, a_2, and κ had been determined in this way the next step was to re-determine the fourth parameter c_3, appearing in the electrostatic energy. By far the most accurate way of doing this is by use of the experimental fission barriers. The calculated barriers for heavy nuclei are very sensitive to the ratio of the electrostatic to the surface energy (or to c_3/a_2) and with a given a_2, the value of c_3 can be determined accurately. Although

some dozens of fission barriers are known or can be estimated, we simplified the fitting problem by requiring only one fission barrier, that of ^{201}Tl, to be reproduced exactly (reasons other than simplicity were also relevant – see subsect. 7.7.). The remaining barriers were used only as a test after the fitting had been completed. In practice the value of the parameter c_3 was changed in steps and the whole fitting procedure for determining the parameters a_1, a_2, κ was repeated until a set of

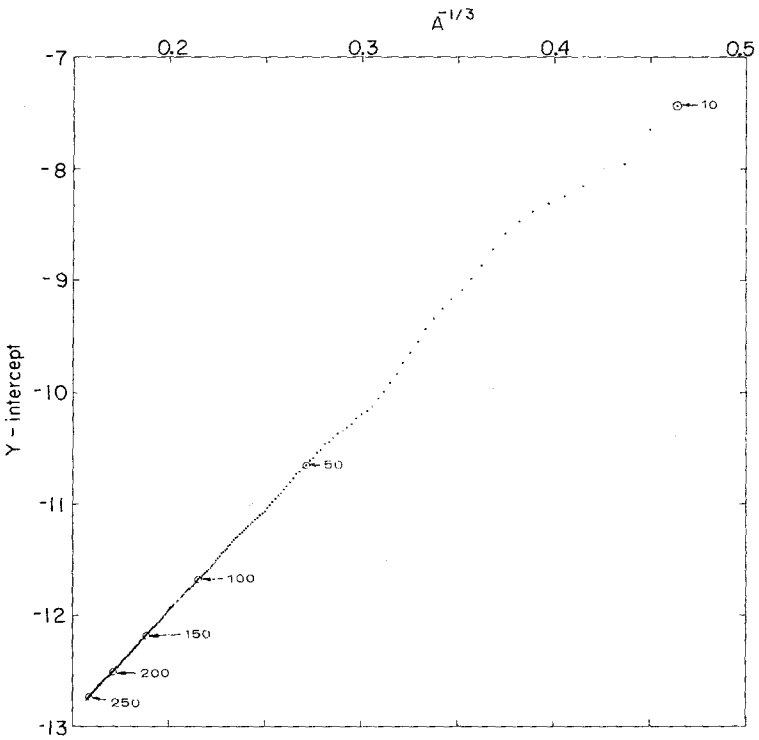

Fig. 12. The Y-intercepts from fig. 9 are plotted against $A^{-\frac{1}{3}}$, to exhibit the linear trend predicted by the liquid-drop formula with volume and surface terms but no curvature correction. The labels on the circled points are A values. Note the false zeros on both the ordinate and abscissa.

parameters a_1, a_2, c_3, κ was obtained which reproduced sufficiently closely the experimental barrier of ^{201}Tl (given as 22.5 ± 1.5 MeV in ref. [17])).

At this stage a new set of liquid-drop parameters was available, and this was used to re-determine the parameters of the shell correction.

6.2. DETERMINATION OF SHELL-CORRECTION PARAMETERS

The new liquid-drop masses were subtracted from the experimental masses. The resulting experimental shell correction ΔE should, according to eq. (9) have the form

$$\Delta E = C\left[\frac{F(N)+F(Z)}{(\frac{1}{2}A)^{\frac{2}{3}}} - cA^{\frac{1}{3}}\right],$$

in the case of *unaeformed* nuclei. Thus if for undeformed nuclei (in practice, nuclei which are *calculated* to be undeformed) the quantity $A^{-\frac{1}{3}}\Delta E$ is plotted against $2^{\frac{2}{3}}[F(N)+F(Z)]/A$, a straight line should result, with C as its slope and $-Cc$ as the intercept on the ordinate axis. An example of such a plot is given in fig. 13.

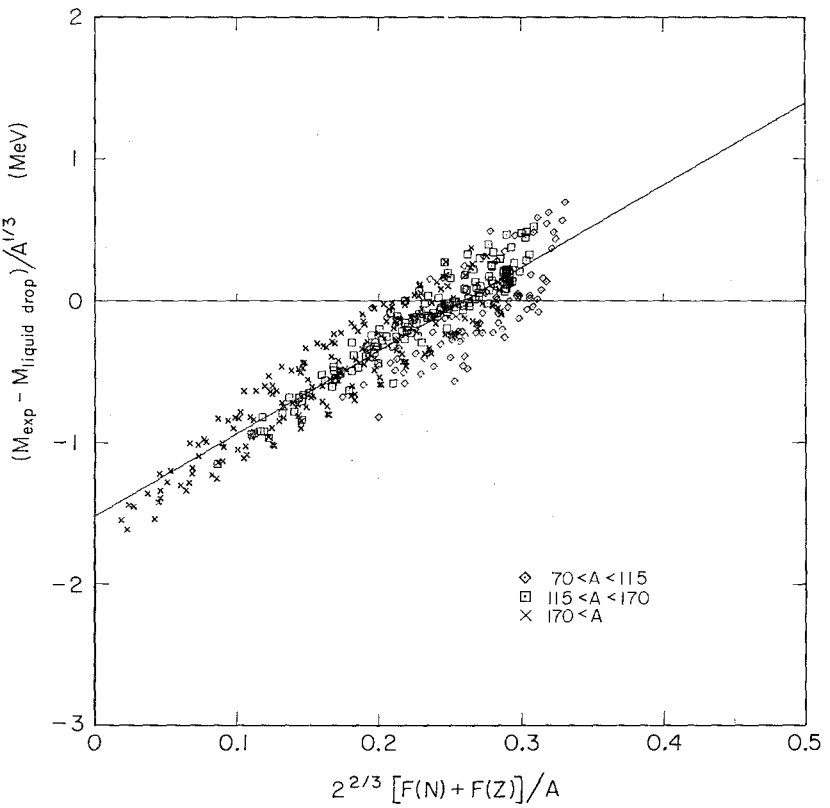

Fig. 13. The experimental shell effects (experimental masses minus calculated liquid-drop masses for undeformed nuclei) were divided by $A^{\frac{1}{3}}$ and plotted against such a function of N and Z that if the functional form of the theoretical shell correction were exact, a straight line would result. For the heavier elements shown in this figure the linear trend is clear. Points for the lighter elements would show much more scatter.

With C and c thus determined, only the range parameter a remained to be fixed. This was done by fitting the calculated quadrupole moments to measured or estimated (intrinsic) quadrupole moments of about 240 nuclei. These were obtained from an unpublished list due to J. C. D. Milton (Atomic Energy of Canada, Ltd., Chalk River, Ontario), based on the values given by Townes [26]) and Okamoto [27]) and supplemented by refs. [28, 29]). In many cases – in particular for the lighter nuclei – the intrinsic quadrupole moments, derived from measurements by means of the formula

(ref. [26]), p. 442)

$$Q(\text{intrinsic}) = \frac{(I+1)(2I+3)}{I(2I-1)} Q(\text{measured})$$

have, at best, only an order-of-magnitude significance, since the conditions for the use of this formula are not satisfied. Even an order-of-magnitude estimate is, however, useful; it shows that there are few strongly deformed lighter nuclei and forces the mass formula to take this into account.

The result of the least-squares fit to the quadrupole moments is illustrated in fig. 23. We may note that by the time the group of 240 experimental quadrupole moments was being fitted, six out of the seven parameters in the mass formula had already been determined from the nuclear masses, so that only *one* parameter was left free to fit the magnitude and structure of the quadrupole moment plot.

The determination of the shell-correction parameters C, c and a completed one cycle of the fitting procedure. The new calculated shell correction was subtracted from experimental masses, new liquid-drop parameters were determined, and the whole cycle was repeated until the seven adjustable parameters had converged to unique values, which they did in a few iterations.

The final values of the parameters are as follows:

$a_1 = 15.677$ MeV,

$a_2 = 18.56$ MeV,

$c_3 = 0.717$ MeV (hence $r_0 = 1.2049$ fm, $c_4 = 1.21129$ MeV),

$\kappa = 1.79$,

$C = 5.8$ MeV,

$c = 0.26$,

$\frac{a}{r_0} = 0.27$.

The mass excess of the hydrogen atom was taken as $M_H = 7.28899$ MeV and of the neutron as $M_n = 8.07144$ MeV. All nuclear mass defects [35]) are on the carbon scale of masses, such that $M(^{12}C) \equiv 0$. (A millimass unit on the carbon scale is related to MeV by 1 mMU = 0.93144 MeV.)

We quote no errors on the seven adjustable parameters in our formula. *Within* the framework of the functional form of our formula the liquid-drop parameters are determined very firmly indeed (say to 1 or 2%) and the shell-correction parameters less firmly, but still adequately (say to 10%–20%). (The best way to get a feeling for how well the parameters are determined is to study figs. 10–13 and 23.) If one goes beyond the framework of our formula (and there may be reasons for that both in the remaining experimental deviations and in theoretical considerations on the

nature of nuclear masses) then the changes in the adjustable parameters will depend on the nature of the new effects taken into consideration and cannot be predicted beforehand.

We note that our value of c_3 predicts the electrostatic energies of nuclei as $E_c = 0.717\, Z^2/A^{\frac{1}{3}} - 1.21129\, Z^2/A$. We have compared energies obtained according to this formula with the electrostatic energies deduced by Hahn *et al.* [32]) from the Stanford electron scattering experiments for $^{40}_{20}$Ca, $^{51}_{23}$V, $^{59}_{27}$Co, $^{115}_{49}$In, $^{122}_{51}$Sb, $^{197}_{79}$Au and $^{209}_{83}$Bi. Our values are consistently lower, by 8.0, 10.3, 8.2, 8.7, 7.8, 7.5 and 5.7%, respectively.

The sizes of these differences suggest a significant effect, which should be investigated.

As regards the values found for the parameters C, c and a, we have already noted in sect. 4 that a is of the order of magnitude expected on the basis of simple considerations. The value of c turns out to be such that the shell correction S is about equally often positive as negative – the average value of S taken over the periodic table would be fairly close to zero (see fig. 6). The basic reason for this result is not clear us.

From the value of C the degree of bunching of the levels in the Fermi gas of sect. 3 may be deduced. Disregarding any velocity dependence of the potential well, the degree of bunching is $C/t_F = 17.5\%$; this is the case illustrated in fig. 3. We can see no reason why the degree of bunching should be the same for all shells, and a closer comparison of the experimental and calculated mass oscillations in figs. 21 and 22 suggests that this is not, in fact, the case. Thus the representation of the region of the doubly magic number at ^{208}Pb would probably be improved if the bunching at $N = 126$ and $Z = 82$ were increased. The need for a different degree of bunching is even more apparent in the light nuclei, where the failure of the original calculated shell correction could be largely removed by an appropriate choice of individual degrees of bunching for the shells at 8, 14, and 28 (with a slight shell at 20); see fig. 16 and subsect. 7.3.

The fact that a constant bunching does represent most of the shell effects fairly well is probably a fortunate accident.

7. Discussion of Results

A glance at fig. 21 or 22 shows the degree of agreement between the experimental and calculated shell oscillations. For nuclei lighter than about $A = 50$ (N about 30) there is practically no correspondence between the calculated shell correction and experiment. [The "microscopic" way of plotting the deviations of nuclear masses from a smooth liquid-drop formula (figs. 21 and 22) should not be allowed to obscure the fact that over-all trends in the binding energies are reproduced well – even for light nuclei. The binding energy of ^{4}He is 28.3 MeV, of ^{56}Fe 492 MeV and of ^{254}Fm 1891 MeV. In relation to these numbers the deviations of a few MeV in fig. 21(c) represent percentage errors decreasing approximately as A^{-1} and no more than 20

to 30 % for He, improving rapidly down to about 1 % in the vicinity of Fe and around 0.1 % for the heavy nuclei – see also fig. 1.] For $A \gtrapprox 50$ there is fair agreement between the calculated and experimental shell corrections, the original shell oscillations in the masses [fig. 21(a)] being cut down by perhaps a factor of five after subtraction of the calculated shell corrections [fig. 21(c)]. The approximate adequacy of the functional form of the shell correction $S(N, Z)$ is seen from fig. 13. This plot, when confined to the not-too-light nuclei, conforms approximately to the expected linear trend.

We shall come back later to a discussion of the remaining deviations between calculation and experiment, including the region of the lighter nuclei, but first we shall consider the degree of success of the liquid-drop part of the formula in representing the general trends of the masses. This question can now be treated with some precision, since the availability of an approximate theoretical shell function enables us to correct the experimental masses for the irregular oscillations associated with magic numbers and, as a result, to deal with a set of masses exhibiting quite a high degree of smoothness.

7.1. SMOOTH TRENDS

This smoothness is well illustrated in figs. 10–12. For the heavier nuclei, in particular, the linearity test of the dependence of the nuclear binding energy on $[(N-Z)/A]^2$ is satisfied with remarkable accuracy. There is no evidence, in this figure, for higher powers of $(N-Z)/A$ at the largest values of the neutron excess; we have not, however, tried to estimate quantitatively the upper limit on the possible amount of such deviations. [Cameron and Elkin [30]) have considered a Gaussian instead of a quadratic symmetry energy, which implies the presence of higher powers of $[N-Z)/A]^2$.]

For the lighter elements in fig. 10 there is more irregularity in the lines connecting isobars. Apart from the irregularities caused by shell oscillations there appears to be present a systematic effect which consistently lowers the points closest to the ordinate axis, indicating some extra binding for nuclei with $N \approx Z$. This light-element anomaly will be isolated and discussed in subsect. 7.2.

We now turn to fig. 11, which tests the assumption of a *constant* (A independent) coefficient in front of the $[(N-Z)/A]^2$ term. A plot of this coefficient against A (fig. 11) reveals some considerable scatter for the lighter elements, related to residual shell effects and to the light-element anomaly mentioned above. For $A \gtrapprox 80$ the scatter is much less and the value of κ is nearly constant, although systematic trends remain, in particular a gradual increase for the heaviest elements. This heavy-element anomaly will be discussed in subsect. 7.4.

We finally come to fig. 12, which shows, as a function of $A^{-\frac{1}{3}}$, a plot of the specifically nuclear binding energy per particle, extrapolated to a "standard nucleus" with $N = Z$. (This extrapolation to $N-Z = 0$ was made by fitting best straight lines through the data in fig. 10, all the lines being *forced* to pass through a common

intercept on the abscissa at the point corresponding to $\kappa = 1.79$, the value adopted on the basis of fig. 11. These straight lines are thus not quite the same as the "best lines" on which fig. 11 is based and which had no restrictions imposed on them.) From fig. 12 we see that the representation of the specifically nuclear energy by means of a volume and a surface term appears to be extremely satisfactory in the range down to $A = 50$. Below $A = 50$ some irregularities appear, as usual, but even down to $A = 10$ one can discern no evidence for a systematic deviation from the straight line that would suggest a higher (the second) power of $A^{-\frac{1}{3}}$. This is of some significance, since a curvature correction to the surface energy (ref. [18])) would appear as a term in the nuclear binding proportional to $A^{\frac{1}{3}}$, which in our plot of binding per particle would show up as a term quadratic in $A^{-\frac{1}{3}}$, introducing a systematic bending of the plot in fig. 12. We have not tried to establish an upper limit on the amount of curvature correction that can be tolerated by the data, and undoubtedly a fair amount could be if all the available parameters were re-adjusted suitably. Still, as things stand, there is no *evidence* in the nuclear masses for a curvature correction. (See appendix A.2 for further remarks on the curvature correction.)

7.2. THE "WIGNER TERM"

For masses below about $A = 50$ our formula fails to reproduce the structure of the experimental mass oscillation in fig. 21. On the one hand the calculated shell function bears no resemblance to the experimental wiggles. On the other a peculiar systematic effect is present in the experimental trends in the neighbourhood of nuclei with $N = Z$. This may be discerned in fig. 21(a) by following a sequence of isotopes with a given Z and noting the behaviour on crossing the point where $N = Z$. In the 21 cases where this can be done ($Z = 2$ to $Z = 22$) there is almost always a kink in the mass at $N = Z$, the mass of such a nucleus being especially low with respect to its neighbours. Alternatively we may make a plot where the mass differences from fig. 21 are plotted as functions of $(N-Z)/A$ for a fixed A, and the break at $N = Z$ is displayed. This break can be seen readily even before the removal of irregularities due to shell structure (which introduces other breaks, at magic numbers N_{magic}, Z_{magic}) but it is brought out most clearly, and its properties can be best studied, if the shell effects are first removed as far as possible. The shell effects for the lighter nuclei are the subject of the next subsection, where a semi-empirical shell function $S(N, Z)$ is derived for these nuclei directly from the experimental values of the masses of nuclei with $N = Z$ (rather than from specific assumptions about the bunching of levels in a Fermi gas). In particular a relative shell correction, i.e., the difference in the shell correction for an isobar with $N \neq Z$ and with $N = Z$, may be deduced.

Applying this method and using the mass differences for $N = Z$ in fig. 21(a), a provisional relative shell correction

$$S_{\text{provisional}}(N, Z) - S(\tfrac{1}{2}A, \tfrac{1}{2}A)$$

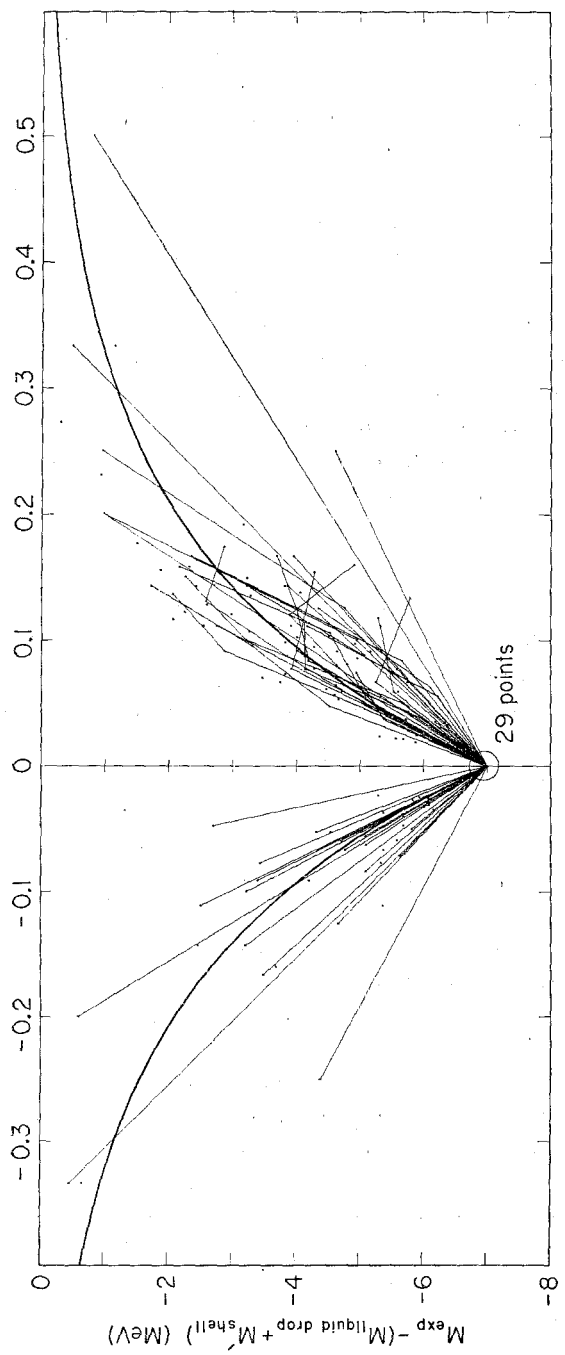

Fig. 14. The sharp trough along $N = Z$, occurring in the masses of the lighter nuclei, is illustrated. The experimental masses in the range $A = 4$ to $A = 58$ were corrected for all known effects (liquid-drop binding and shell effects deduced from nuclei with $N = Z$) and the remainder plotted as a function of $(N-Z)/A$. Lines connect even mass isobars, dots correspond to odd values of A. The smooth curve is the exponential function $-7\exp(-6|N-Z|/A)$.

was deduced. This semi-empirical correction was applied to the experimental mass differences in fig. 21(a), leaving a remainder term which represents what is left over after allowing for all the expected contributions to nuclear binding (which include all the conventional liquid-drop terms as well as the most nearly realistic correction for shell effects that we could devise). This remainder was plotted as a function of $(N-Z)/A$ and, expect for a change in the zero in the ordinate scale, is shown in fig. 14. In this plot we have collected 28 isobaric curves for $A = 4$ to $A = 58$, all suggesting a kink at $N = Z$. Each curve shows the behaviour of the mass as one moves away from the point $N = Z$. Masses *relative* to the mass of the nucleus with $N = Z$ are shown, so that all the points for $N = Z$ coincide. This common point appears at the value of -7 MeV along the ordinate for a reason that will be explained below.

The plot in fig. 14 shows that, in addition to any shell effects that may be producing breaks at special values of N or Z, one can discern a sharp-angled "trough" or "crease" in the mass surface along the locus $N = Z$. Both sides of this trough can be seen in the range from $A = 4$ to $A = 42$ and traces of one of its sides can be discerned in fig. 10 up the values of A around 60 to 80.

We have speculated on the origin and significance of this additional binding energy of nuclei with $N \approx Z$. We believe it is related to the so-called Wigner term which, under certain assumptions, exhibits the characteristic "kinked" dependence on the absolute magnitude $|N-Z|$. (See refs. [19, 20]), and also chapt. VII, p. 271 of ref. [21])). A sharp dependence on $|N-Z|$ seems to be demanded by the data. The physical interpretation of such a term is not clear to us, and the functional dependence of any new term in the mass formula designed to represent it is not obvious. We do not believe, however, that an expression simply proportional to $|N-Z|$ is suitable, on two accounts. First, the plot in fig. 10 suggests rather a correction to the straight lines that *dies out* with increasing values of $(N-Z)/A$. Second, we surmise that the additional binding energy for $N = Z$ is somehow related to the identity of the neutron and proton wave functions in such nuclei. This would result in a particularly good overlap of the wave functions – a matching of the nodes and antinodes (or the density distributions) of the neutrons and protons – and would indeed be expected to lead to a somewhat tighter interaction between them than is the case on the *average*. (There is an analogy here with the pairing interaction for particles in time-reversed orbits.) If this *average* is taken to mean something like the case of a large amorphous mixture of neutron and proton Fermi gases, without special phase relations between the wave functions of the two, then with respect to this average the additional stability associated with $N = Z$ should be a function with a limited range in $N = Z$, disappearing when N and Z differ sufficiently to destroy the special phase relationships (the extra overlap) responsible for the extra binding. We are using here an argument analogous to that according to which shell effects should vanish with distortion: in the average, or amorphous, state of nuclear matter there are no special symmetries or degeneracies, either in space or as regards neutron and proton

numbers. Any extra binding associated with such symmetries should therefore be damped out as these symmetries disappear (see sect. 4).

In view of these considerations we have tentatively represented the extra binding displayed in fig. 14 by means of a short-range (exponential) function

$$\Delta E_{\text{Wigner}} = -7 \exp\left(-6\left|\frac{N-Z}{A}\right|\right) \text{MeV}.$$

The two parameters (amplitude -7 MeV and range 6 of the exponential) are chosen, on the one hand, to reproduce the trend of the points in fig. 14 and, on the other, to insure the disappearance of the effect for larger values of $(N-Z)/A$. We sl refer to this additional binding term as the Wigner term, although its form differs from the conventional one.

The experimental mass deviations in fig. 21(a) were now corrected with the Wigner term ΔE_{Wigner}, and the remainder was subjected to the procedure of analysing the masses into a liquid-drop part and a shell correction along the lines of sect. 6. (The re-fitted values of a_1, a_2 and κ are equal to 15.7546 MeV, 19.1015 MeV and 1.78, respectively. The parameter c_3 was not re-fitted.) The final effect of including the Wigner term is illustrated by a comparison of figs. 15(b) and 15(c). In the former, which is identical with fig. 21(a), the mass deviations show, as noted before, no correspondence with the calculated shell correction in fig. 21(b). In fig. 15(c) allowance for the Wigner term has made the remainder resemble more nearly what one would expect from a shell correction associated with magic numbers – this is discussed in the next subsection.

We have not proceeded with the systematic incorporation of the Wigner term into our formula, and a re-fitting of all constants, because of inadequate information on its true functional form. In particular the dependence of this additional binding on the shape of a nucleus is unknown. These important questions will have to be investigated theoretically before the Wigner term, for whose existence there is clear evidence, can be incorporated satisfactorily in a mass formula.

7.3. SHELL FUNCTION FOR $N, Z \leqq 29$

Our calculated shell function $S(N, Z)$ is quite incapable of reproducing the experimental shell oscillations for the lighter nuclei. Fortunately, in the special case when masses of nuclei with $N = Z$ are known, it is possible to deduce directly a semi-empirical two-dimensional function $S(N, Z)$ from the one-dimensional empirical function $S(\frac{1}{2}A, \frac{1}{2}A)$. Thus, if we retain the functional form of our shell correction

$$S(N, Z) = C\left[\frac{F(N)+F(Z)}{(\frac{1}{2}A)^{\frac{4}{3}}} - cA^{\frac{1}{3}}\right],$$

then, without claiming to be able to calculate the function F from first principles, we

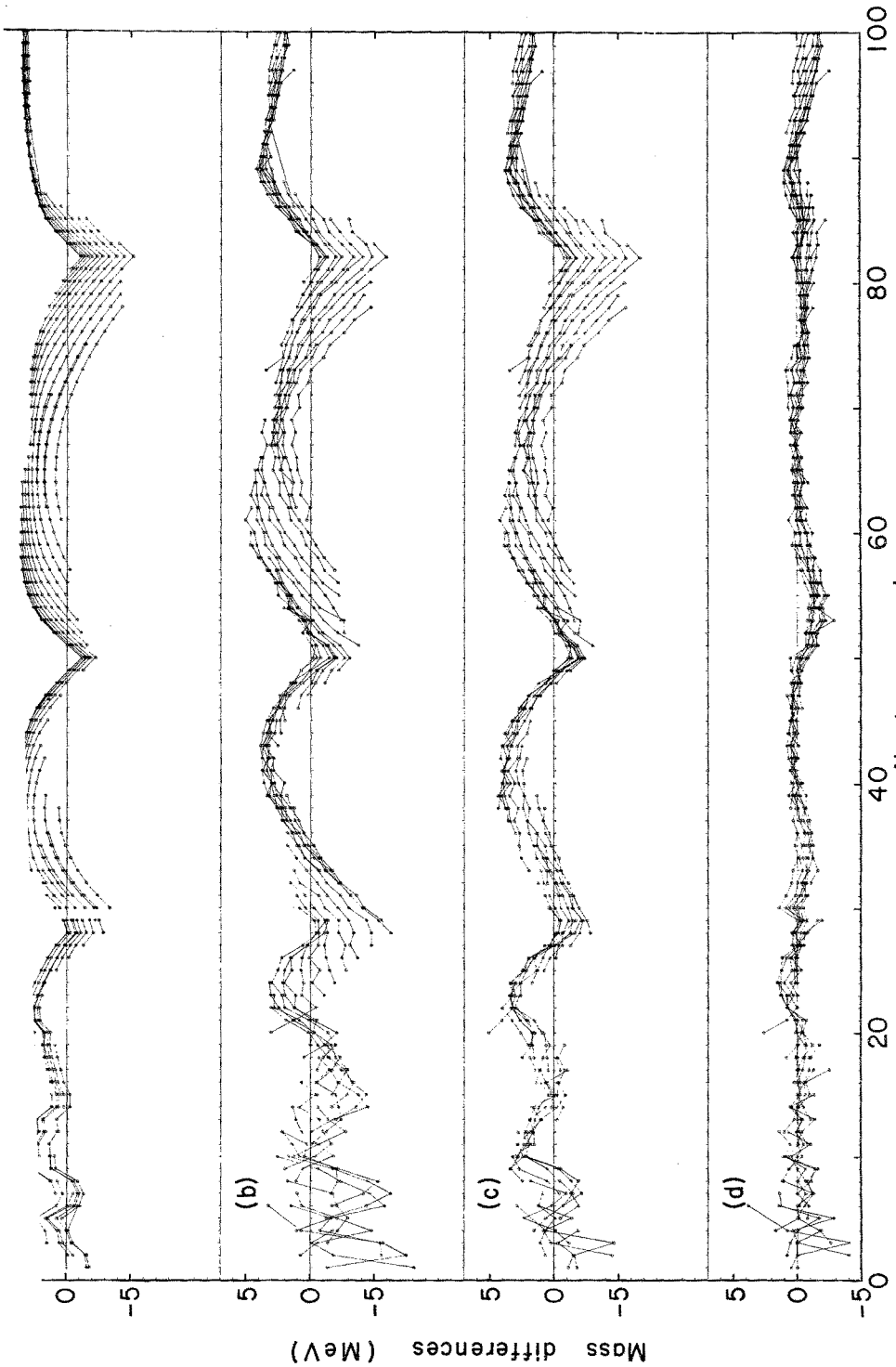

Fig. 15. These plots refer to different treatments of the deviations of nuclear masses from a liquid-drop formula in the region of the lighter nuclei. All plots are against neutron number, with lines connecting isotopes. The top figure illustrates the shell correction calculated from a bunched Fermi gas (to the right of the break at $N = 29$) or from empirical masses of nuclei with $N = Z$ (to the left). (b) is a plot of the experimental deviations from a liquid-drop formula (with the constants arrived at in sect. 6), and (c) shows the effect of the Wigner Term (the liquid-drop constants were refitted). This is now the experimental shell correction to be compared with the semi-empirical one in line (a). The difference between (a) and (c) is shown in (d).

may yet deduce the following relation:

$$S(N, Z) = \frac{1}{2} \frac{N^{\frac{2}{3}} S(N, N) + Z^{\frac{2}{3}} S(Z, Z)}{(\frac{1}{2}A)^{\frac{2}{3}}} . \tag{16}$$

[This is readily obtained by writing down the expressions for $S(N, Z)$, $S(N, N)$ and $S(Z, Z)$ and eliminating $F(N)$ and $F(Z)$].

TABLE 1

Shell function derived from the masses of nuclei with equal numbers of neutrons and protons

Particle number X	$S(X, X)$ (MeV)
1	−1.779
2	−1.506
3	0.238
4	0.709
5	2.364
6	−0.693
7	−1.329
8	−0.449
9	2.714
10	2.807
11	2.835
12	1.640
13	1.895
14	−0.261
15	−0.231
16	0.656
17	1.053
18	1.568
19	1.872
20	1.707
21	3.240
22	3.230
23	2.583
24	1.698
25	0.770
26	−0.160
27	−1.305
28	−2.846
29	−2.214

We shall use this relation to predict masses of nuclei with $N \neq Z$ on the basis of the masses of nuclei with $N = Z$. The physical meaning of this procedure is that we are still considering the shell correction to be due to an identical bunching of levels for neutron and proton Fermi gases in a common potential well, but instead of trying to calculate the bunching we determine it directly from the empirical masses of nuclei with $N = Z$. The derivation of formula (16) disregards the possible presence of deformed nuclei and, strictly speaking, does not apply to such cases. In practice,

however, the formula will, by definition, reproduce the masses of nuclei with $N = Z$, whether these are deformed or not. Any errors will be proportional to the degree of extrapolation away from $N = Z$, which is not large for the cases of interest.

The 29 experimental values for $S(X, X)$ in table 1 were taken from the calculation on which fig. 15(c) is based. That is, these values are the result of starting with the experimental mass deviations in fig. 21(a); correcting them for the Wigner term; re-fitting the liquid-drop parameters a_1, a_2 and κ (but not c_3) and displaying the remaining deviations as an experimental shell correction $S(N, Z)$. Formula (16)

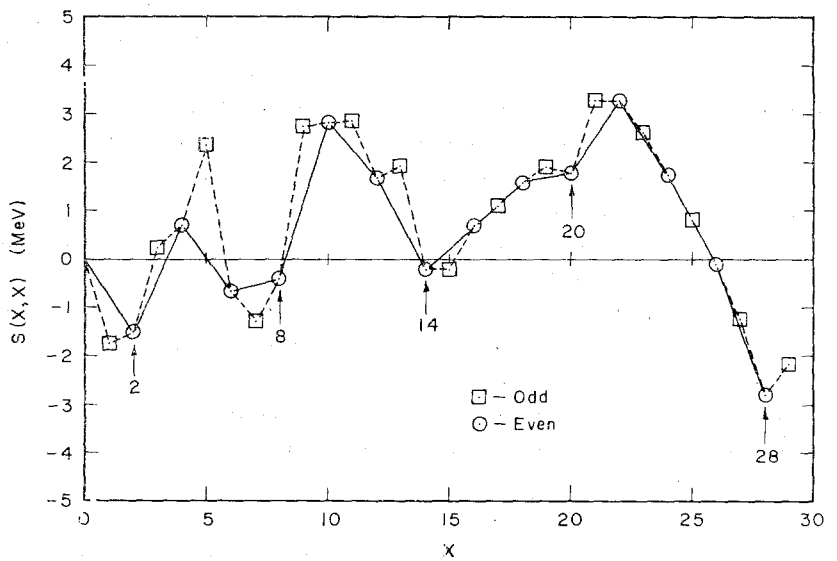

Fig. 16. The empirical shell correction $S(X, X)$ is shown as a function of X. The solid line connects even points only, the dashed line connects all points. Special binding may be attributed to the numbers 2, 8, 14, 28, with a slight dip at 20.

was then used to construct the left-hand part of fig. 15(a). The right-hand part is the conventionally calculated shell correction, the same as in fig. 21(b). Fig. 15(a) shows the predicted shell effect and is to be compared with fig. 15(c). The difference between the two is shown in fig. 15(d).

We note that in the semi-empirical shell correction for $N, Z \leqq 29$ (fig. 15(a)) the irregularities associated with magic numbers are rather less, in absolute magnitude, than for the heavier nuclei. The shell at $N, Z = 20$ is hardly discernible, although there is a slight change of slope there. A somewhat bigger break seems to be present around $N, Z = 14$ and there is another dip, or change of slope, close to $N, Z = 8$. (In locating such dips one should in general connect by lines only nuclei of the same type: even, odd or odd-mass. The fact that the even-odd correction $\delta = 11/A^{\frac{1}{2}}$ MeV is not quite accurate introduces some spurious irregularities between neighbouring points in plots of the type of fig. 15. Thus the mass at $N = Z = 7$ appears to be

lower than at $N = Z = 8$). Fig. 16 shows a plot of the one-dimensional function $S(X, X)$, in which the breaks at magic numbers are somewhat more clearly displayed. The fact that, on the basis of nuclear masses, a shell effect at 14 is more pronounced than at 20 is noteworthy.

7.4. HEAVY-ELEMENT ANOMALY

One of the more easily discernible systematic deviations in figs. 21(c) or 22(c) is the tendency of the experimental mass differences to become progressively lower with increasing Z, for elements beyond about radium. The effect amounts to about 3 to 4 MeV between $Z = 88$ and $Z = 102$ and is quite a smooth function of Z. A very slight effect of this nature is present in the calculations [see fig. 21(b) or 22(b)] and is associated with the increasing softness of heavy nuclei against deformation, but the calculated trend is several times smaller than the observed. We have been unable to prove or disprove any of a number of hypotheses as to the origin of the trend. This effect had been noticed several times before [22, 38]), also in connection with the somewhat anomalous location of the valley of β-stability for heavy nuclei, which is one of its consequences. Another way of describing it is to say that it tends to contribute to the stability of the heavier elements, by depressing their ground-state masses. The reality of this interpretation is confirmed by the near-constancy of measured fission barriers between thorium and americium. The gain of some 3 to 4 MeV in the stability of the ground states tends to compensate for the greater fissility of the heavier elements (a lowering of the saddle-point masses) that would be expected on the basis of the liquid-drop theory. The degree to which the heavy-element anomaly explains the constancy of the fission barriers is discussed in subsect. 7.7 and fig. 17. In any case the indications are that the anomaly must be some effect associated with the ground-state equilibrium shapes and one which disappears when the nucleus in question is distorted into a saddle-point configuration. Such behaviour would be expected from a shell effect, although the gradual decrease of the masses with Z is unlike any of the shell effects that our semi-empirical treatment would predict.

7.5. THE RARE-EARTH ANOMALY

It has been pointed out to us by Dr. F. Stephens of this Laboratory that the decrease of masses in the region $Z \approx 88$ to $Z \approx 102$ is paralleled, though to a reduced degree, in the same general range of neutron numbers, $N \approx 88$ to $N \approx 112$ (the rare-earths). This lends weight to the hypothesis that perhaps both effects *are* associated with irregularities in single-particle level spacings characteristic of the nuclear potential.

In the case of the rare earths there appears to be a connection between the failure of our formula to follow in detail the masses and its failure to follow in detail the quadrupole moments (fig. 23). At the beginning of the region of large deformations ($N \approx 88$) the experimental masses and the experimental quadrupole moments are both unusually high. On the other hand, towards the end of the region of deforma-

tions, the observed decrease of masses and quadrupole moments is more gradual than the calculated decrease. The quadrupole moments in particular are not well reproduced in the region between the heavy rare earths and the region of the ^{208}Pb shell.

7.6. QUADRUPOLE MOMENTS

The experimental quadrupole moments in fig. 23 are reproduced in a rough way, the root-mean-square deviation being about 1.2 b. According to our formula, nuclei with $N \approx 60$ and $N \approx 40$ have just become deformed, although the deformations are not very large and would probably not lead one to expect the existence of clear rotational spectra for these nuclei (see subsect. 7.9 and ref. [25])). Better rotors would be expected for nuclei closer to the centres of the relevant rectangles in fig. 5.

We note that our mass formula always predicts *positive* quadrupole moments. This is entirely the result of the cubic term in the liquid-drop part of the formula, the shell correction having been taken independent of the nature of the deformation. The cubic term in the liquid-drop formula is relatively less important for the lighter nuclei; the energy difference between oblate and prolate shapes is then smaller and relatively minor effects, neglected in our treatment, could reverse the balance in favour of oblate shapes. It is perhaps significant in this connection that nuclei with observed negative quadrupole moments are confined to the lighter half of the periodic table.

7.7. FISSION BARRIERS

Our formula may be used, in principle, for the calculation of fission saddle-point shapes and barriers. Since, however, fission barriers are small differences of larger quantities, it is especially important to be aware of the limitations of our formula when applying it to the calculation of barriers.

In table 2 we have collected 39 measured or estimated fission barriers and compared them with barriers calculated in two somewhat different ways. In both cases the saddle-point mass was calculated by means of our formula, but the ground state was either taken from experiment (column headed semi-empirical barrier) or from our mass formula (column headed calculated barrier). In cases where an experimental ground-state mass is available, or can be reliably extrapolated from neighbouring nuclei, the first way of estimating a fission barrier should be more reliable, since it treats at least the bottom of the barrier correctly, the only error arising in estimating the top (the saddle-point mass).

We see from table 2 that with the electrostatic energy parameter c_3 adjusted to reproduce approximately the barrier of ^{201}Tl (see sect. 6 – the "semi-empirical" value of 22.418 is to be compared with the measurement of 22.5 ± 1.5 MeV) the overall trend of fission-barrier heights is reproduced by the calculation. In particular the high fission barriers between ^{201}Tl and ^{213}At in the range 22 to 16 MeV are followed from ^{232}Th on, by much lower barriers, of the order of 5 to 6 MeV and less. This

TABLE 2

Fission barriers

Nucleus	x	Experimental barrier	Liquid-drop barrier	Semi-empirical barrier	Calculated barrier
^{201}Tl	0.6761	22.5±1.5 [b])	17.438	22.418	21.328
^{207}Bi	0.6914	20.6±2 [c])	14.924	22.145	21.484
^{209}Bi	0.6889	20.6±2 [c])	15.365	23.900	23.497
^{210}Po	0.6991	18.6±2 [c])	13.763	21.006	21.136
^{213}At	0.7068	15.8±2 [c])	12.674	16.242	17.543
^{232}Th	0.7410	5.95 [d])	8.642	5.183	6.774
^{233}Th	0.7400	6.44 [d])	8.752	5.303	6.856
^{232}Pa	0.7520	6.18 [d])	7.552	4.555	5.740
^{233}U	0.7620	5.49 [d])	6.652	4.288	4.873
^{234}U	0.7608	5.2 [e])	6.756	4.243	4.950
^{235}U	0.7597	5.75 [d])	6.858	4.246	5.027
^{236}U	0.7587	5.8 [e])	6.957	4.138	5.105
^{237}U	0.7576	6.4 [d])	7.054	4.424	5.184
^{238}U	0.7566	5.80 [d])	7.148	4.154	5.262
^{239}U	0.7557	6.15 [d])	7.240	4.157	5.340
^{237}Np	0.7686	5.49 [d])	6.116	3.789	4.311
^{238}Np	0.7675	6.04 [d])	6.209	3.983	4.386
^{236}Pu	0.7810	4.7 [a])	5.160	3.173	3.452
^{238}Pu	0.7786	4.9 [a])	5.343	3.425	3.593
^{239}Pu	0.7775	5.48 [d])	5.432	3.599	3.664
^{240}Pu	0.7764	4.7 [e])	5.520	3.313	3.737
^{241}Pu	0.7753	6.3 [e])	5.605	3.527	3.808
^{242}Pu	0.7743	4.9 [a])	5.688	3.253	3.880
^{244}Pu	0.7723	4.8 [a])	5.848	3.186	4.022
^{241}Am	0.7864	6.00 [e])	4.807	3.182	3.086
^{242}Am	0.7852	6.4 [e])	4.887	3.248	3.152
^{240}Cm	0.7989	4.3 [a])	3.999	2.744	2.379
^{242}Cm	0.7965	4.4 [a])	4.157	2.844	2.504
^{244}Cm	0.7941	4.4 [a])	4.309	2.711	2.630
^{246}Cm	0.7919	4.5 [a])	4.454	2.744	2.755
^{248}Cm	0.7899	4.4 [a])	4.593	2.635	2.880
^{249}Bk	0.7997	4.6 [a])	3.979	2.453	2.337
^{246}Cf	0.8143	4.0 [a])	3.160	2.429	1.636
^{248}Cf	0.8119	4.0 [a])	3.290	2.471	1.743
^{250}Cf	0.8097	4.1 [a])	3.416	2.417	1.852
^{252}Cf	0.8075	3.8 [a])	3.537	1.931	1.960
^{253}Es	0.8174	4.2 [a])	3.019	1.743	1.522
^{254}Es	0.8164	4.2 [a])	3.074	1.596	1.572
^{254}Fm	0.8274	3.5 [a])	2.554	1.713	1.143

[a]) Barriers estimated from the empirical relation

$$\text{barrier} = \tfrac{1}{8}[29+\log_{10} t_{\frac{1}{2}}(\text{years})] \text{ MeV}.$$

The factor $\frac{1}{8}$ is a conversion factor from the logarithm of a half-life (measured in units of a characteristic nuclear period, about 10^{-29} y) to MeV, obtained by taking the average value of the ratio of the barrier to the half-life for six nuclei for which both quantities have been measured (^{234}U, ^{235}U, ^{236}U, ^{237}U, ^{239}Pu and ^{240}Pu). The half-lives were obtained from the reference in footnote [d]).

[b]) Ref. [17]). [c]) Ref. [40]).
[d]) Ref. [41]). [e]) Ref. [42]).

rather sudden decrease of the barriers is associated with the decreased stability of nuclei beyond the doubly magic ^{208}Pb region (see fig. 17).

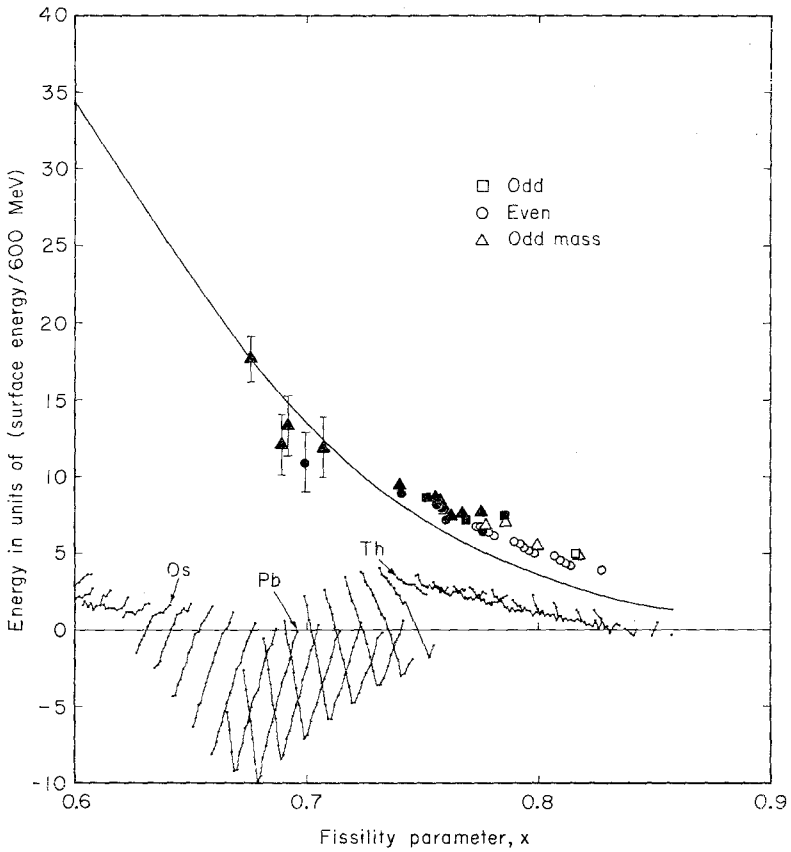

Fig. 17. This figure compares experimental and calculated saddle-point masses. All masses are plotted with respect to a smooth reference surface, the mass of a spherical liquid drop. The energies are in units of the surface energy of the drop, in order to make the saddle-point mass a function of one variable, the fissility parameter x instead of both N and Z. (The factor of 600 MeV, included in the units of the ordinate, is of the order of the surface energy of a heavy nucleus and makes a unit on the vertical scale approximately equal to one MeV). The smooth line is the calculated curve, equal to 600 $\xi(x)$. Closed symbols indicate measured barriers while open symbols are used for barriers which are inferred from half-lives. The normalizing point ^{201}Th is on the left. The lower part of the figure shows the behaviour of the ground-state mass deviations for the heavy elements, with lines connecting isotopes. Note the heavy-element anomaly. The difference between the ground-state mass and the saddle mass is a fission barrier.

A fair amount of experimentation with various choices of the adjustable parameters has shown that beyond a rough account of the over-all trends, our treatment is still unable to reproduce in detail the behaviour of the observed fission barriers. In particular the calculated barriers for elements heavier than thorium are too low

and decrease too rapidly with increasing Z. By a slight change of c_3 the absolute magnitude of the barriers could easily be increased by the required 1 or 2 MeV (introducing, however, a disagreement with the measurement for ^{201}Tl), but the calculated barriers would still decrease too rapidly with Z. The too-slow decrease of

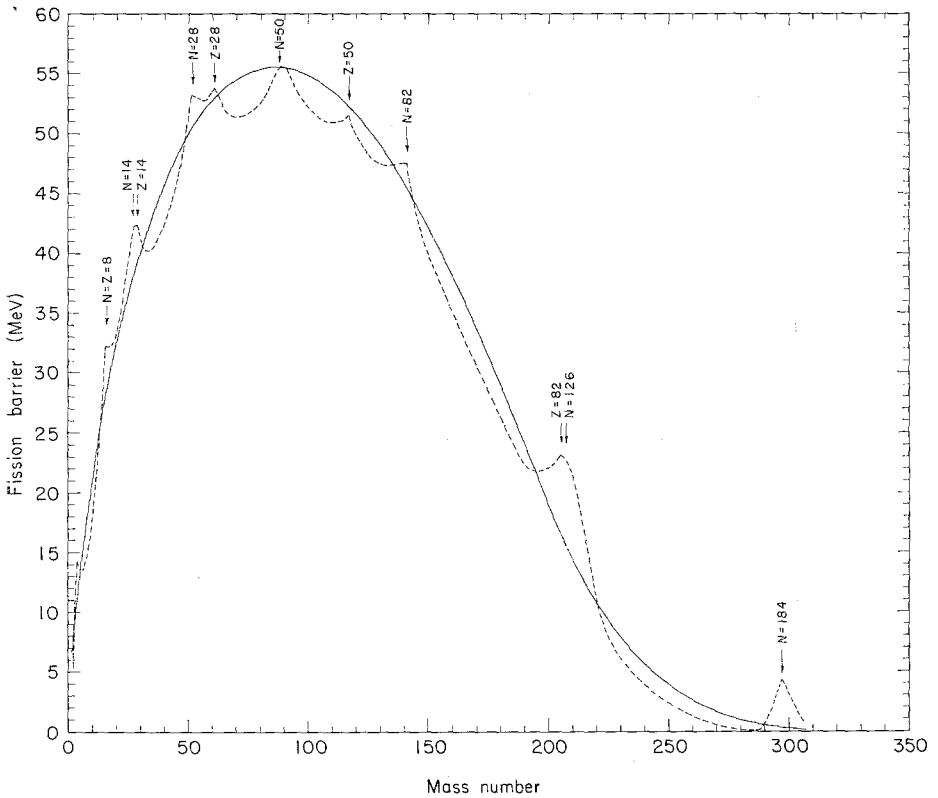

Fig. 18. The fission barrier energy, in MeV, is shown for nuclei along Green's approximation to the valley of stability. The smooth curve is the liquid-drop result; the irregular dashed curve is calculated from our mass formula and shows shell effects. Nuclei with $N \approx 50$ ($A \approx 90$) should require the greatest amount of energy for their disintegration, lighter and heavier elements being more easily disrupted into comparable fragments.

experimental fission barriers with Z (or with the fissility parameter x) is a puzzle of long standing. As may be seen from fig. 17 the "heavy-element anomaly" – the systematic decrease of the mass deviations of the heavy elements – helps to remove the really drastic discrepancy with a pure liquid-drop calculation of fission barriers, but, apparently, the heavy-element anomaly is not the whole explanation of the barrier problem. (In table 2 the liquid-drop barrier decreases from 8.6 MeV for ^{232}Th to 2.6 MeV for ^{254}Fm, a difference of 6.1 MeV. In the column headed semi-empirical barrier, the corresponding decrease is from 5.2 MeV to 1.7 MeV or 3.5

MeV. The decrease estimated from experiment is 5.2 MeV–3.4 MeV or 1.8 MeV only.)

It was partly because we felt that the problem of fission barriers is still not completely understood (perhaps especially for the heavy elements where the puzzle of fission asymmetry is also present) that we did not try to obtain least-squares fits to all barrier measurements but chose the simple procedure of fitting only ^{201}Tl. The resulting discrepancy in the barriers of the heavier elements tends then to underline the fact that a difficulty still exists in the interpretation of the fission barriers to within an accuracy of 1 or 2 MeV.

For the purposes of an over-all survey of fission barriers throughout the periodic table, our mass formula may turn out to be more nearly adequate. We have plotted in fig. 18 fission barriers for elements along the valley of stability. The smooth curve corresponds to the liquid-drop approximation and the irregular curve shows the effects of shells (in this figure the shell effects were calculated rather than taken from experimental ground state masses). Note that the barriers go through a maximum of about 55 MeV in the region of $A \approx 90$. (This is also the region where fission should cease to be distinguishable from fragmentation and the conventional symmetric saddle-point looses its significance as a fission barrier – see ref. [7])). Note also the region around $x \approx 1$ ($A \approx 300$), where the fission barriers, after becoming vanishhingly small, rise once again to values of several MeV. This is an illustration of the effect on nuclear stability of hypothetical magic numbers beyond the end of the periodic table, which we shall now discuss.

7.8. SUPER-HEAVY NUCLEI

In our mass formula we have included, for purposes of illustration, magic numbers at $Z = 126$ and $N = 184$, 258 – see fig. 19. (The latter numbers are obtained by following the sequence of major shells in a harmonic oscillator potential with spin-orbit coupling). We do not wish to imply that there are grounds for believing that any of these magic numbers would show up in practice, and we use them only to illustrate what some of the consequences would be if a magic number turned out to be present in the general neighbourhood of super-heavy nuclei somewhat beyond the end of the periodic table. The actual values of the magic numbers might be different; for example, we have recently learned [23]) that $Z = 114$, $N = 184$ is a possible candidate for a doubly magic nucleus (see also p. 269, ref. [24])). What we wish to point out is that *if* a (doubly) magic number exists then an important consideration affecting the possible stability of the corresponding nucleus is the considerable increase in the barrier against fission and, consequently, in the spontaneous fission half-life. This is illustrated in fig. 2 where we have plotted the deformation energy predicted by our mass formula for the case $Z = 126$, $N = 184$. This nucleus has a fissility parameter $x = 1.05$; as a result, in the absence of shell effects, it would have a vanishing barrier against fission and a spontaneous fission half-life of the order of nuclear collective oscillations or 10^{-22} sec. Because of the assumed doubly magic

number, however, the ground-state mass of this nucleus would be depressed (by about 10.2 MeV according to our formula). Since this depression is, according to our treatment, a rapidly decreasing function of deformation, there results a considerable barrier against fission, with a height of 9.0 MeV: the extra binding associated with the doubly magic number has stabilized the otherwise highly fissile nucleus. An

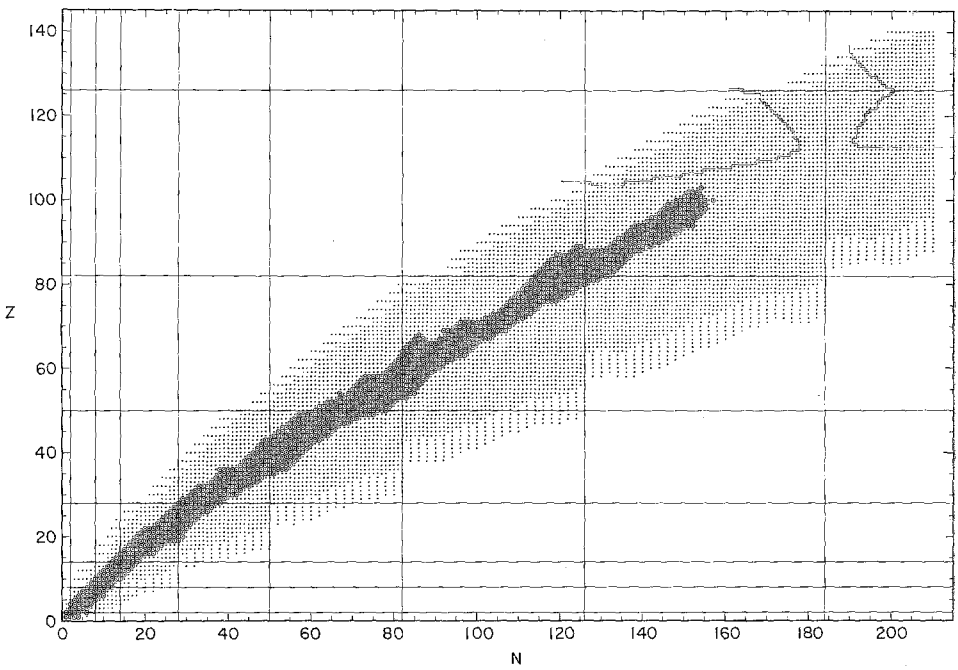

Fig. 19. Nuclei whose masses are known are shown as circles, nuclei included in the table of nuclear properties in ref. [39]) are indicated by dots. The lower boundary of the dots is the neutron "drip line" (the neutron binding energy vanishes there). The upper boundary is an approximate indication of the proton drip line, taken to be the line where a proton becomes unbound by more than 3 MeV. The tasseled appearance of the boundaries is the result of the even-odd term in the binding energy. Note the magic-number lines. The irregular, thin line in the upper right-hand corner is the fission or "split line", i.e., the boundary where the (calculated) fission barrier vanishes. The hypothetical doubly magic number at $N = 184$, $Z = 126$ causes this line, which would otherwise be almost horizontal, to make an excursion upwards, around the doubly magic nucleus.

estimate of the spontaneous fission half-life of such a nucleus would involve a discussion of the *width* (as well as the height) of the barrier. We expect the width to be much smaller than for conventional heavy nuclei and hence even with the high fission barrier the half-life for spontaneous fission might or might not turn out to be in the range where such a super-heavy nucleus would be accessible to experimental study (for example, in suitable heavy-ion reactions). In order to proceed in a realistic manner with a discussion of the existence and location of possible islands of stability

beyond the periodic table the first requirement is the availability of estimates for the location and strength of magic number effects in that region. When such estimates have become available (through single-particle calculations in realistic nuclear potentials) it will be possible to apply our semi-empirical treatment of nuclear masses and deformations to the prediction of the fission barriers of hypothetical superheavy nuclei (as well as to estimates of the neutron, proton and alpha binding energies that may be relevant to their stability).

7.9. CENTRIFUGAL STRETCHING OF NUCLEI

Our mass formula is meant to treat, in the first place, only *static* properties of nuclei. By adding to it a rotational energy, however, one may attempt to predict certain gyrostatic properties, i.e., the properties of a system in uniform rotation. Attempts along these lines are described in ref. [25]). The centrifugal energy is there taken in the form $\frac{1}{2}$(angular momentum)^2/(moment of inertia), where the moment of inertia is assumed to be an increasing function of nuclear deformation; for example, proportional to the square of the deformation parameter β or σ. The sum of this rotational energy and of the potential energy taken from the mass formula, when minimized with respect to deformation, may be used to study the centrifugal stretching of nuclei and leads to predictions of characteristic spacings of rotational energy levels.

7.10. HOW TO USE THE MASS FORMULA

We would like to end this section with remarks on what we would consider to be the legitimate use of our mass formula. Since the formula attempts to provide a semi-empirical theory of the deformabilities of nuclei throughout the periodic table with the aid of no more than seven adjustable parameters, it is out of the question that the details of the 1200 masses, 240 quadrupole moments and 40 fission barriers should be reproduced accurately: The immediate consequence is that in extrapolating the masses, quadrupole moments or fission barriers only a small distance away from regions where these properties are known experimentally, it is by far the best procedure to make use of the experimental values themselves. In such cases our mass formula may have only a secondary use. For example, to extrapolate nuclear masses, it would be more convenient, and perhaps more accurate, to extrapolate the *differences* between experimental masses and our formula, rather than the masses themselves.

For somewhat more distant extrapolations the gain in using our formula may become more important. For example, the trends of the experimental masses on leaving the region of the closed shell at ^{208}Pb, if extrapolated indiscriminately into the rare earths or actinides, would lead to quite incorrect (excessively high) masses. If, instead, the extrapolations were made on the differences between experimental and calculated masses, no gross errors would result, because the change of trend in the masses associated with the onset of deformed nuclei would be allowed for, albeit only approximately.

For distant extrapolations – say half-way across a shell – the use of our mass formula *without* reference to experimental masses might be the most adequate procedure (because the experimental mass deviations might be only local irregularities which ought not to be extrapolated too far). However, as with all extrapolations, a very generous margin of error should be allowed for. Finally, for extremely distant extrapolations, it should be remembered that any predictions associated with shell effects must start with a knowledge of the locations and strengths of magic numbers, a question that is outside the framework of our treatment, which assumes the magic numbers as given. For such very distant extrapolations the only significant part of our mass formula would be the liquid-drop aspect.

In summary, our formula should be used with caution and, whenever possible, in conjunction with directly available experimental information.

Appendix D of ref. [39]) contains a table of calculated masses and other nuclear properties for some 8000 particle-stable nuclei.

8. Summary and Conclusions

This paper has been concerned with a semi-empirical theory of the nuclear potential-energy surface considered as a function of the nuclear shape. Our theory regards this energy surface as given by an average, asymptotic, liquid-drop behaviour, modified by local shell corrections in the form of "dimples". The liquid-drop part of the energy, with four adjustable parameters, consists of volume and surface energies (both composition-dependent) and a Coulomb energy. The shell-correction dimples are Gaussian functions specified in terms of bunched neutron and proton Fermi gases and have three adjustable parameters.

The body of experimental data to be compared with our theory refers to static properties of nuclei. It consists of some 1200 nuclear ground-state masses, some 240 quadrupole moments and some 40 fission barriers. These data are sufficient to give a firm determination of all the adjustable parameters. An over-all comparison of theory with experiment confirms the adequacy of the liquid-drop formula for representing the trends of nuclear binding energies. A detailed comparison of the calculated and experimental shell correction reveals a general correspondence, except for nuclei with mass numbers less than 50, where a more adequate treatment of the shell correction is necessary and appears possible. After this is done there remains, apart from minor deviations, one systematic difference between theory and experiment, for which a new term in the mass formula is suggested. It is characterized by additional binding of nuclei with equal or nearly equal neutron and proton numbers and is recognizable as a sharp trough along the locus of nuclei where $N = Z$. This additional contribution to the nuclear binding energy appears to be related to earlier discussions of a "Wigner term". We have expressed it tentatively in the form $-7 \exp[-6|(N-Z)/A|]$ MeV.

After correcting the experimental masses for shell effects and for the Wigner term,

the remaining binding energy is a smooth function of N and Z, which is represented with astonishing faithfulness by a simple liquid-drop formula, for all nuclei throughout the periodic table from $A \approx 4$ to $A \approx 260$. There are no systematic trends left over to suggest the need for appreciable higher-order corrections to the expansion in powers of $A^{-\frac{1}{3}}$ on which the liquid-drop formula is based or for a more complicated representation of the dependence of the binding on nuclear composition. The values found for the adjustable parameters in the liquid-drop part of the formula are not very different from earlier determinations, for example Green's [1]). Because shell effects and fission barriers are taken into account in our fits, the coefficients are more firmly established, however. Also, the connection that our theory suggests between nuclear masses and deformations has enabled us to provide an answer to the question of how the separation between shell oscillations and the smooth liquid-drop trends should be made.

The account which our theory gives of the shell oscillations and of the quadrupole moments is only rough and there is room for improvement.

To summarize: our treatment is a first step beyond the liquid-drop theory of nuclear masses and deformabilities and represents an intermediate stage between this simple theory and the detailed but complicated microscopic investigations of the deformabilities of individual nuclei. The price we pay in going beyond the liquid-drop model is the introduction of a Gaussian function and three adjustable parameters. The gain is a rough semi-quantitative understanding of the shell oscillations, quadrupole moments, and fission barriers. A by-product is the isolation of the Wigner term and the re-assessment of the accuracy of the liquid-drop formula.

The problems raised by our analysis of nuclear masses and deformations have to do, first, with a better interpretation of the semi-empirical regularities we have observed and, second, with an analysis of the remaining deviations. In the first class of problems we would put a better analysis of the expected functional form of the attenuating factor, first and foremost perhaps its γ-dependence. The theoretical significance of the base-line parameter c should be clarified. The physical origin and functional form of the Wigner term, including the question of its shape dependence, must also be settled. As regards discrepancies, the rare-earth and heavy-element anomalies should be studied further, the latter in particular being of importance for an understanding of fission barriers and for extrapolations of nuclear properties beyond the end of the periodic table. The reason for the 5 to 10% discrepancies of the electrostatic energies with the Stanford values should be investigated.

Finally we would like to make a remark concerning a problem that goes beyond the scope of a study of nuclear potential energies but which forms a complement to such a study. The basic reason why the understanding of a potential-energy surface is of importance is that this energy, written out as a function of the degrees of freedom specifying the system, constitutes one half of a Hamiltonian function. The other half of the Hamiltonian is the kinetic energy, written out as a function of the coordinates and the conjugate momenta. In order to have a complete theory of a system both

parts of the Hamiltonian must be known. In the case of the dynamical liquid-drop model the kinetic-energy part of the Hamiltonian is well known and understood. Studies of the effects of nuclear shell structure on the deviations of the kinetic energy from its liquid-drop value would constitute a complement to the study of the deviations of the potential energy. If one were fortunate enough to find a semi-empirical account of the kinetic energy deviations as simple as our treatment of the potential energy, one would be in possession of a compact semi-empirical Hamiltonian on the basis of which an approximate account of some of the simpler aspects of nuclear dynamics might be built.

We would like to thank S. Bjørnholm, F. S. Stephens, R. M. Diamond, S. G. Thompson, S. Johansson, H. Kümmel, J. C. D. Milton, H. Meldner and P. Röper for discussions and correspondence; and H. Kümmel, J. Mattauch, W. Thiele and A. H. Wapstra for permission to use their tabulations of experimental nuclear masses prior to publication.

Appreciation is expressed to Jeannette Mahoney for able assistance with the early computations and plots.

Appendix

A.1. DETAILS OF EQUILIBRIUM DEFORMATIONS

A.1.1. *The onset of deformations.* Confining ourselves to axially symmetric spheroidal shapes ($\gamma = 0$), we discuss the solutions of the equilibrium condition, eq. (11) in sect. 5. This equation may be re-written as

$$\theta - \tfrac{3}{2}\varepsilon\theta^2 - v\theta e^{-\theta^2} = 0,$$

where ε is the small quantity F/E and v an abbreviation for S/E or S/S_{crit}. The above equation is satisfied by $\theta = \theta_0 = 0$ or by

$$1 - \tfrac{3}{2}\varepsilon\theta = v e^{-\theta^2}. \tag{17}$$

Taking logarithms of both sides, expanding the left-hand side in powers of ε, and retaining the first power, we find the following quadratic equation for θ

$$\theta^2 - \tfrac{3}{2}\varepsilon\theta - \ln v = 0.$$

There are two solutions, θ_+ and θ_-

$$\theta_\pm = \tfrac{3}{4}\varepsilon \pm [(\tfrac{3}{4}\varepsilon)^2 + \ln v]^{\frac{1}{2}}. \tag{18}$$

The onset of deformations is given by the condition

$$(\tfrac{3}{4}\varepsilon)^2 + \ln v > 0,$$

which is nearly, but not quite, the condition for the loss of stability of the sphere,

$$\left.\frac{\partial^2 M}{\partial \theta^2}\right|_{\theta=0} < 0,$$

which leads to $\ln v > 0$ (see sect. 5). Deformed equilibrium shapes in fact occur for the first time when $\ln v$ is slightly negative, i.e., when S is a little less than S_{crit}, and the *sphere is still stable*. The pair of deformed equilibrium shapes θ_+ and θ_- start off at the *finite* (though small) value $\theta_+ = \theta_- = \frac{3}{4}\varepsilon$, after which θ_+ increases and θ_- decreases rapidly (with a vertical tangent). At this stage there are thus three equilibrium shapes: the sphere and θ_+, both stable, and θ_-, an unstable barrier

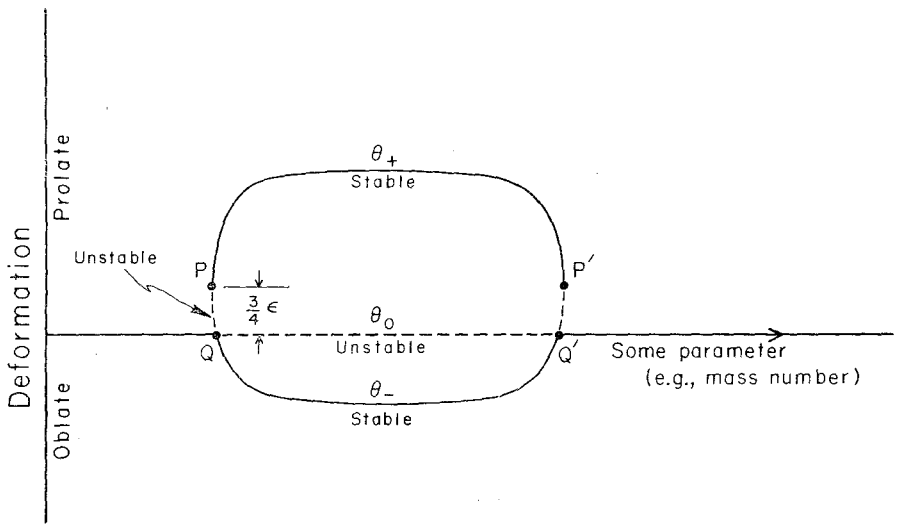

Fig. 20. This figure illustrates schematically the details of the appearance and disapearance of deformations according to our mass formula. Non-spherical equilibrium shapes θ_+ and θ_- appear first at the limiting point P and the sphere loses stability almost immediately after, at the bifurcation point Q, where θ_- and θ_0 cross. At Q′ the sphere regains stability and at P′ deformations disappear through the annihilation of θ_+ and θ_-. Solid lines indicate stability (against axially symmetric deformations), dashed lines indicate instability.

between them (see fig. 20). The sphere loses stability at the point Q in fig. 20 at the moment when the family of solutions denoted by θ_- crosses the family θ_0 of spherical solutions. This is a typical example of Poincaré's "exchange of stabilities". [Using the terminology of, for example, Appell's textbook – ref. [8]), Vol. 4, chapt. VIII, P is a "limiting point" and Q is a "point of bifurcation."] Beyond the point Q the sphere is unstable and θ_-, which now corresponds to oblate deformations, is stable with respect to axially symmetric deformations (though not otherwise – see sect. 5). At the end of the region of deformations the sequence of events in fig. 20 is reversed, with the sphere regaining stability at Q′ and deformations disappearing at P′. The

general appearance of a plot of the equilibrium families θ_+ and θ_- is that of a television screen, whose horizontal axis is displaced by the amount $\frac{3}{4}\varepsilon$ above the line of spheres $\theta_0 = 0$.

In practice the range of A values between P and Q, and P′ and Q′ is so extremely small that in our numerical studies we did not come across a single example of a nucleus exhibiting simultaneous stability of the sphere and of a deformed shape. This means that in eq. (18) we may neglect the narrow range of conditions when $(\frac{3}{4}\varepsilon)^2$ cannot be regarded as small compared to $\ln v$ and the square root has to be left unexpanded. Apart then from this small neighbourhood close to the critical condition $\ln v \approx 0$, we may neglect the $(\frac{3}{4}\varepsilon)^2$ term in the radical and rewrite eq. (18) as

$$\theta_\pm = \pm(\ln v)^{\frac{1}{2}} + \tfrac{3}{4}\varepsilon,$$

which is the result used in sect. 5.

A.1.2. *Saddle-point shapes.* Eq. (17) has, as a rule, a solution corresponding to a fission saddle-point. When this occurs for values of θ of the order of unity, so that the term $\exp(-\theta^2)$ cannot be neglected, a numerical treatment of eq. (17) may be resorted to. Because the range of our attenuating function corresponds to quite small nuclear eccentricities, the retention of only the quadratic and cubic terms in the liquid-drop part of our formula is then quite adequate even for saddle-point shapes. When the saddle-point occurs for values of θ well beyond the range of the attenuating function, the liquid-drop part of the energy cannot be expanded in powers of the eccentricity, and, in any case, it is essential not to restrict the shape of the drop to spheroidal distortions. On the other hand the shell correction term $\exp(-\theta^2)$ can then be neglected altogether and the saddle-point shape is given by the condition that the liquid-drop part of the energy be stationary with respect to all small distortions – a problem whose solution is known (e.g., refs. [7, 33]). In order to decide in practice whether to use the large-θ approximation (shell effects neglected) or the small-θ approximation (a spheroidal drop treated to cubic order) one may calculate the saddle-point energy in three different ways and on this basis decide whether the neglect of shell effects or the neglect of trans-cubic terms introduces the more serious error. Thus one may solve eq. (17) with and without the shell term, obtaining an estimate of the error ΔE_1, say, associated with the neglect of shell effects (the large-θ approximation). Then, for the same nucleus one may calculate the pure liquid drop saddle point energy both exactly and in the "cubic approximation" [i.e., spheroidal shapes, energy to order θ^3 – in other words, once again eq. (17) with the shell term neglected]. From this comparison one may obtain an estimate of the error ΔE_2, say, associated with the cubic or small-θ approximation.

If $\Delta E_1 > \Delta E_2$, one may use the small-θ approximation [eq. (17)]; if $\Delta E_1 < \Delta E_2$, one may use the large-θ approximation (the pure liquid drop). In practice the liquid-drop approximation is good for all nuclei up to a value of the fissility parameter of about 0.925, and the smaller of the errors ΔE_1 or ΔE_2, does not exceed, at worst, a few hundredths of an MeV.

A.2. DIFFUSENESS AND CURVATURE CORRECTIONS

We shall prove two theorems, one relating to the diffuseness correction to the electrostatic energy, the other to the curvature correction to the surface energy.

A.2.1. *Diffuseness correction.* The change in electrostatic energy δE_c, resulting from changing an arbitrarily shaped sharp distribution ρ_{sharp} into a diffuse one ρ_{diffuse} is an integral over all space of the old electrostatic potential v times the change in the charge density $\delta\rho$, given by $\rho_{\text{diffuse}}-\rho_{\text{sharp}}$. (We assume this difference to be effectively confined to a small region in the vicinity of the old surface and to be a function of the normal distance n from the surface but not of the location on the surface. It follows that for any point on the surface the integral $\int \mathrm{d}n\delta\rho$ must vanish if charge is to be conserved.) Thus

$$\begin{aligned}
\delta E_c &= \int_{\text{space}} v\delta\rho \\
&= \int \mathrm{d}n \oint \mathrm{d}\sigma\, v\delta\rho \\
&= \int \mathrm{d}n \oint \mathrm{d}\sigma \left[v(n=0)+\left(\frac{\partial v}{\partial n}\right)_0 n+\ldots\right]\delta\rho \\
&= \oint \mathrm{d}\sigma\, v(0)\int \mathrm{d}n\,\delta\rho+\int \mathrm{d}n\, n\delta\rho \oint \mathrm{d}\sigma \left(\frac{\partial v}{\partial n}\right)_0+\ldots .
\end{aligned}$$

In the last two lines we have made a Taylor expansion of the electrostatic potential in powers of the normal distance from the old surface. The first term vanishes because $\int \mathrm{d}n\,\delta\rho = 0$. Carrying out the surface integration in the second term and applying Gauss' theorem in electrostatics, we find

$$\delta E_c = -4\pi(\text{total charge})\int_{-\infty}^{\infty} \mathrm{d}n\, n\delta\rho.$$

The change in energy is thus, to this order in the diffuseness of the surface, strictly independent of the *shape* of the charge distribution. Applying our formula to a diffuseness of the charge distribution given by a Woods-Saxon (or Fermi) form factor

$$\rho_{\text{diffuse}}(n) = \rho_0 \frac{1}{1+\mathrm{e}^{n/d}},$$

we find the result, quoted in ref. [16]) and used in sect. 5:

$$\delta E_c = -\tfrac{1}{2}\pi^2 \frac{e^2}{r_0}\frac{Z^2}{A}\left(\frac{d}{r_0}\right)^2.$$

Since this term is independent of nuclear shape, the shape-dependence of the electrostatic energy is still that of a *sharp* distribution. It follows that the fissility parameter x, which for a sharp distribution may be defined as the ratio of the electrostatic energy of a sphere to twice the surface energy, becomes, for a diffuse distribution, the ratio of *what the electrostatic energy would be if the distribution were sharp* to twice the surface energy.

Thus

$$x = (c_3 Z^2/A^{\frac{1}{3}})/(2c_2 A^{\frac{2}{3}}),$$

and not

$$[c_3 Z^2/A^{\frac{1}{3}} - c_4 Z^2/A]/(2c_2 A^{\frac{2}{3}}).$$

A.2.2. *Curvature correction.* In general the specific surface tension γ may be a function of the local curvature of the surface κ, given by $(R_1^{-1}+R_2^{-1})$, where R_1 and R_2 are the principal radii of curvature of the surface at the point in question (ref. [18]). Making a Taylor expansion in powers of κ, we may write

$$\begin{aligned}\text{specific surface tension} &= \gamma(\kappa = 0) + \left(\frac{\partial\gamma}{\partial\kappa}\right)_0 \kappa + \ldots \\ &= \gamma + \gamma'\kappa = \gamma(1+l\kappa),\end{aligned}$$

where $l = \gamma'/\gamma = \mathrm{d}(\ln\gamma)/\mathrm{d}\kappa$ is the logarithmic derivative of γ with respect to κ, a quantity with the dimensions of a length. The surface energy in this case of a curvature-dependent surface tension is thus

$$E_s = \oint_S \mathrm{d}\sigma\gamma(1+l\kappa),$$

where the integral is over the surface S of the shape in question. On inspection of the above expression we realize that it is identical with the integral

$$\oint_{S_{new}} \mathrm{d}\sigma_{new}\gamma,$$

where the new surface is obtained from the old one by a *normal outward shift* through the distance l. (If the old element of area is written out as $\mathrm{d}\sigma_{old} = R_1\mathrm{d}\theta R_2\mathrm{d}\phi$, where θ and ϕ are two orthogonal angular coordinates specifying a point on the surface, we have

$$\begin{aligned}d\sigma_{new} &= (R_1+l)\mathrm{d}\theta(R_2+l)\mathrm{d}\phi = R_1\mathrm{d}\theta R_2\mathrm{d}\phi[1+l(R_1^{-1}+R_2^{-1})+\ldots] \\ &= \mathrm{d}\sigma_{old}(1+l\kappa),\end{aligned}$$

which proves our statement.) Hence we have the theorem that the surface energy in the case of a curvature-dependent surface tension is equal to the surface energy for a *constant* surface tension but calculated for a new surface, displaced normally by

an amount equal to the logarithmic derivative of the specific surface tension with respect to curvature.

This theorem helps to visualize the effect of a curvature-dependent surface tension – for example, in its effect on nuclear fission. It also enables one to combine this correction with a further correction that is of some interest, namely the correction for a *true* difference in the locations of the nuclear matter and charge surfaces (see ref. [34])). (The effective location of the surface relevant for calculating a surface energy is then the true difference augmented by l.)

We may summarize this section by the statement that if we have a *diffuse* charge distribution and a matter distribution whose surface is *outside* the charge distribution by a normal distance b, and which moreover gives rise to a *curvature-dependent* surface tension, then, as regards the shape dependence of its energy this complicated system may be replaced by the simpler one of a *sharp* charge distribution, and a matter distribution with a *constant* surface tension but displaced normally by the sum of b and l. The fissility parameter x is in this case the ratio of the electrostatic energy of a sharp spherical charge distribution (of radius R, say) to twice the simple surface energy of a sphere of radius $(R+b+l)$.

A.3. FOLD-OUT FIGURES

In this appendix we have collected the three figures which, because or their size, would be cumbersome in the body of the text.

References

1) A. E. S. Green, Nuclear Physics (McGraw-Hill, New York, 1955) especially chapt. 9
2) M. Baranger and K. Kumar, Nuclear Physics **62** (1965) 113;
   S. Das Gupta and M. A. Preston, Nuclear Physics **49** (1963) 401
3) B. R. Mottelson and S. G. Nilsson, Mat. Fys. Skr. Dan. Vid. Selsk. **1**, No. 8 (1959);
   D R. Bès, Mat. Fys. Skr. Dan. Vid. Selsk. **32**, No. 2 (1961);
   D. R. Bès and Z. Szymański, Nuclear Physics **28** (1961) 42
4) E. Marshalek, L. W. Person and R. K. Sheline, University of California Lawrence Radiation Laboratory Report UCRL-10364 (July 1962)
5) F. S. Mozer, Phys. Rev. **116** (1959) 970
6) H. Kümmel, J. H. E. Mattauch, W. Thiele and A. H. Wapstra, in Proc. Conf. on Nuclidic Masses, Vienna, 1963, ed. by W. H. Johnson, Jr. (Springer-Verlag, Wien-New York, 1964) p. 42
7) S. Cohen and W. J. Swiatecki, Ann. of Phys. **22** (1963) 406
8) H. Lamb, Hydrodynamics, 6th ed. (Dover Publications, New York, 1945), sects. 377, 378; P. Appell, Mecanique rationnelle vol. 4, Part 1 (Gauthier-Villars, Paris, 1932) chapt. 8, sects. 97–102;
   R. A. Lyttelton, The stability of rotating liquid masses (Cambridge University Press, Cambridge, 1953) chapt. 2;
   S. Cohen and W. J. Swiatecki, Ann. of Phys. **19** (1962) 67
9) W. J. Swiatecki, Phys. Rev. **104** (1956) 993; in Proc. Second United Nations Int. Conf. on the Peaceful Uses of Atomic Energy, Geneva, 1958 (United Nations, Geneva, 1958) Paper P/651
10) S. G. Nilsson, Mat. Fys. Medd. Dan. Vid. Selsk. **29**, No. 16 (1955)
11) V. F. Weisskopf, Revs. Mod. Phys. **29** (1957) 174
12) A. H. Wapstra, in Handbuch der Physik, ed. by S. Flügge, Vol. 38/1 (Springer-Verlag, Berlin, 1958) p. 1

13) V. G. Nossoff, in Proc. Int. Conf. on the Peaceful Uses of Atomic Energy, Geneva, 1955 (United Nations, New York, 1956) Report A/CONF. 8/P/653 USSR
14) D. L. Hill and J. A. Wheeler, Phys. Rev. **89** (1953) 1102, especially pp. 1124 and 1125
15) B. C. Carlson, J. Math. Phys. **2** (1961) 441
16) W. J. Swiatecki, in Proc. Conf. on Nuclidic Masses, Vienna, 1963, ed. by W. H. Johnson, Jr. (Springer-Verlag, Wien-New York 1964) p. 58
17) D. S. Burnett *et al.*, Phys. Rev. **134** (1964) B952
18) V. M. Strutinskii and A. S. Tyapin, JETP (Soviet Physics) **18** (1964) 664; ZhETP (USSR) **45** (1963) 960;
V. M. Strutinskii, The shape of a fissioning nucleus at the saddle point and the liquid drop model of the nucleus, preprint, I. V. Kurchatov Institute of Atomic Energy, Moscow (1964)
19) E. Feenberg and E. P. Wigner, Phys. Rev. **51** (1937) 95
20) E. Wigner, Phys. Rev. **51** (1937) 947
21) J. M. Blatt and V. F. Weisskopf, Theoretical Nuclear Physics (John Wiley & Sons, New York, 1952)
22) R. A. Glass, S. G. Thompson and G. T. Seaborg, J. Inorg. Nucl. Chem. **1** (1955) 3–44;
A. E. S. Green and D. F. Edwards, Phys. Rev. **91** (1953) 46–53, fig. 4
23) H. Meldner and P. Röper (Institut für Theoretische Physik der Universität Frankfurt/M.) personal communication (1965)
24) M. A. Preston, Physics of the nucleus (Addison-Wesley Publ. Co., Reading, Massachusetts, 1962)
25) R. M. Diamond, F. S. Stephens and W. J. Swiatecki, Phys. Lett. **11** (1964) 315–318
26) Charles H. Townes, in Handbuch der Physik, Vol. 38/1, ed. by S. Flügge (Springer-Verlag, Berlin, 1958) p. 377
27) K. Okamoto, Phys. Rev. **110** (1958) 134
28) United States Atomic Energy Commission, 1960 Nuclear Data Tables, Part 4 (U.S. Government Printing Office, Washington 25, D.C.)
29) D. R. Bès and Z. Szymański, Nuclear Physics **28** (1961) 42; Zdzislaw Szymański, *ibid.* **28** (1961) 63
30) A. G. W. Cameron and R. M. Elkin, Role of the symmetry energy in atomic mass formulas (Goddard Institute for Space Studies, New York,)
31) W. J. Swiatecki, Proc. Phys. Soc. **A64** (1951) 226
32) B. Hahn, D. G. Ravenhall and R. Hofstadter, Phys. Rev. **101** (1956) 1131
33) V. M. Strutinsky, N. Ya. Lyashchenko and N. A. Popov, Nuclear Physics **46** (1963) 639–659
34) Th. A. J. Maris, Phys. Rev. **101** (1956) 147–148
35) J. H. E. Mattauch, W. Thiele and A. H. Wapstra, Nuclear Physics **65** (1965) 1
36) J. R. Nix, Ph. D. theses, Lawrence Radiation Laboratory UCRL-11338 (April 1964);
J. R. Nix and W. J. Swiatecki, Nuclear Physics **71** (1965) 1
37) James J. Griffin, in Proc. Int. Atomic Energy Agency Symposium on the Physics and Chemistry of Fission, Salzburg, Austria, March 1965, to be published
38) W. J. Swiatecki, Phys. Rev. **101** (1956) 97–99
39) W. D. Myers and W. J. Swiatecki, Lawrence Radiation Laboratory Report UCRL-11980 (May 27, 1965)
40) J. R. Huizenga, R. Chaudhry and R. Vandenbosch, Phys. Rev. **126** (1962) 210
41) E. K. Hyde, The nuclear properties of the heavy elements, Part III, Fission Phenomena (Prentice-Hall, Englewood Cliffs, New Yersey, 1964) p. 23
42) I. Halpern, Ann. Rev. Nucl. Sci. **9** (1959) 245–342